

# WRF-Chem simulated surface ozone over South Asia during the pre-monsoon: Effects of emission inventories and chemical mechanisms

Amit Sharma<sup>1, 2, \*</sup>, Narendra Ojha<sup>2, \*</sup>, Andrea Pozzer<sup>2</sup>, Kathleen A. Mar<sup>3</sup>, Gufran Beig<sup>4</sup>, Jos Lelieveld<sup>2, 5</sup>, and Sachin S. Gunthe<sup>1</sup>

<sup>1</sup>Department of Civil Engineering, Indian Institute of Technology Madras, Chennai, India

<sup>2</sup>Atmospheric Chemistry Department, Max Planck Institute for Chemistry, Mainz, Germany

<sup>3</sup>Institute for Advanced Sustainability Studies, Potsdam, Germany

<sup>4</sup>Indian Institute for Tropical Meteorology, Pune, India

<sup>5</sup>Energy, Environment and Water Research Center, The Cyprus Institute, Nicosia, Cyprus

\*Correspondence to: Amit Sharma ([amit.iit87@gmail.com](mailto:amit.iit87@gmail.com)) and Narendra Ojha ([narendra.ojha@mpic.de](mailto:narendra.ojha@mpic.de))

## Abstract

We evaluate numerical simulations of surface ozone mixing ratios over the South Asian region during the pre-monsoon season, employing three different emission inventories (EDGAR-HTAP, INTEX-B, and SEAC4RS) in the WRF-Chem model with the RADM2 chemical mechanism. Evaluation of diurnal variability in modelled ozone compared to observational data from 15 monitoring stations across South Asia shows the model ability to reproduce the clean, rural and polluted urban conditions over this region. In contrast to the diurnal average, the modelled ozone mixing ratios during noontime i.e. hours of intense photochemistry (1130-1630 h Indian Standard Time or IST) are found to differ among the three inventories. This suggests that evaluations of the modelled ozone limited to 24-h average are insufficient to assess uncertainties associated with ozone build-up. HTAP generally shows 10-30 ppbv higher noontime ozone mixing ratios than SEAC4RS and INTEX-B, especially over the north-west Indo-Gangetic Plain (IGP), central India and southern India. The HTAP simulation repeated with the alternative MOZART chemical mechanism showed even more strongly enhanced surface ozone mixing ratios due to vertical mixing of enhanced ozone that has been produced aloft. Our study indicates the need to also evaluate the O<sub>3</sub> precursors across a network of stations and the development of high-resolution regional inventories for the anthropogenic emissions over South Asia accounting for year-to-year changes to further reduce uncertainties in modelled ozone over this region.

## 1. Introduction

Tropospheric ozone plays central roles in atmospheric chemistry, air quality and climate change. Unlike primary pollutants, which are emitted directly, tropospheric ozone forms photochemically involving precursors such as carbon monoxide (CO), volatile organic compounds (VOCs) and oxides of nitrogen (NO<sub>x</sub>), supplemented by transport from the stratosphere (e.g. Crutzen, 1974; Atkinson, 2000; Monks et al., 2015). It can be transported over long distances resulting in enhanced concentrations even in areas located remote from the sources of precursors (Cox et al., 1975). The photochemical production of ozone and its impacts on agricultural crops and human health are especially pronounced near the surface. Numerous studies have shown that elevated surface ozone levels significantly reduce crop yields (e.g.; Krupa et al., 1998; Emberson et al., 2009; Ainsworth et al., 2012; Wilkinson et al., 2012), in addition to adverse human health effects that cause premature mortality (e.g., Bell et al., 2004; Jerrett et al., 2009; Anenberg et al., 2010; Lelieveld et al., 2015).

An accurate representation of anthropogenic emissions of ozone precursors is essential to understand the photochemical production of ozone and support policy making. While anthropogenic emissions have been nearly stable or decreasing over northern America and Europe (e.g. Yoon and Pozzer, 2014), there has been substantial enhancement over the East and South Asian regions in recent decades (e.g. Akimoto, 2003; Ohara et al., 2007, Logan et al., 2012; Gurjar et al., 2016). The number of premature mortalities per year due to outdoor air pollution is anticipated to double by the year 2050 as compared to the year 2010 in a business-as-usual scenario, predominantly in Asia (Lelieveld et al., 2015). The multi-pollutant index over all populated regions in the northern hemisphere shows a general increase, with South Asia being the major hotspot of deteriorating air quality (Pozzer et al., 2012).

The growth of anthropogenic emissions over the South Asian region has regional implications, and is also predicted to influence air quality on a hemispheric scale (Lelieveld and Dentener, 2000). It was shown that the anthropogenic emissions and their subsequent photochemical degradation over South Asia influence air quality over the Himalayas (e.g. Ojha et al., 2012; Sarangi et al., 2014) and the Tibetan Plateau (Lüthi et al., 2015) as well as the marine environment downwind of India (e.g. Lawrence and Lelieveld, 2010). Additionally, the prevailing synoptic scale weather patterns make this region highly conducive to long-range export of pollutants (e.g. Lelieveld et al., 2002; Lawrence et al., 2003; Ojha et al., 2014; Zanis et al., 2014). Therefore, the accurate estimation of anthropogenic emissions over South Asia and their representation in chemical transport models are essential to quantify the effects on regional as well as global air quality.

The Weather Research and Forecasting model with Chemistry (WRF-Chem) (Grell et al., 2005; Fast et al., 2006), a regional simulation system, has been popular for use over the South Asian region in numerous recent studies to simulate the meteorology and spatio-temporal distribution of ozone and related trace gases (e.g. Kumar et al., 2012a, 2012b; Michael et al., 2013; Gupta et al., 2015; Jena et al., 2015; Ansari et al., 2016; Ojha et al., 2016; Girach et al., 2017). WRF-Chem simulations at higher spatial resolution employing regional emission inventories have been shown to better reproduce the observed spatial and temporal heterogeneities in ozone over this region as compared to the global models (e.g. Kumar et al., 2012b; Ojha et al., 2016). However, an evaluation of modelled ozone based on data from a network of stations across South Asia is imperative considering very large spatio-temporal heterogeneity in the distribution of ozone over this region (e.g. Kumar et al., 2010; Ojha et al., 2012; Kumar et al., 2012b) mainly resulting from heterogeneous precursor sources and population distribution. WRF-

Chem simulated ozone distributions have also been utilized to assess the losses in crop yields, and it was suggested that the estimated crop losses would be sufficient to feed about 94 million people living below the poverty line in this region (Ghude et al., 2014). Further, WRF-Chem has been used to estimate that premature mortality in India caused by chronic obstructive pulmonary disease (COPD) due to surface O<sub>3</sub> exposure was ~12,000 people in the year 2011 (Ghude et al., 2016). Despite these applications, there is room for improvement in modeled concentrations as some limited studies evaluating ozone on diurnal scales revealed a significant overestimation of noontime ozone e.g. by as much as 20 ppbv in Kanpur (Michael et al., 2013) and 30 ppbv in Delhi (Gupta and Mohan, 2015).

Using WRF-Chem, Amnuaylojaroen et al. (2014) showed that over continental southeast Asia surface ozone mixing ratios vary little (~4.5%) among simulations employing different emission inventories. A recent study by Mar et al. (2016) highlighted the dependence of WRF-Chem predicted ozone air quality (over Europe) on the chosen chemical mechanism. These results indicate the need for evaluating the effects of emission inventories and chemical mechanisms on the model performance using a network of stations across South Asia, which has not been carried out thus far. The main objectives of the present study are:

- (a) To evaluate WRF-Chem simulated ozone over South Asia, especially the diurnal variability, against recent in situ measurements from stations representing different chemical environments (urban, rural, clean etc.);
- (b) To inter-compare model simulated O<sub>3</sub> among different emission inventories;
- (c) To inter-compare model simulated O<sub>3</sub> between two extensively used chemical mechanisms (MOZART and RADM2) with the same emission inventory;

We focus on the pre-monsoon season (March-May) for the study as O<sub>3</sub> mixing ratios at the surface are generally the highest over most of South Asia during this period (Jain et al., 2005; Debaje et al., 2006; Reddy et al., 2010; Ojha et al., 2012; Gaur et al., 2014; Renuka et al., 2014; Bhuyan et al., 2014; Sarangi et al., 2014; Yadav et al., 2014; Sarkar et al., 2015). This is because photochemistry over South Asia is most intense during this season caused by the combined effects of high pollution loading, biomass-burning emissions and a lack of precipitation. The effects of biomass burning on ozone in Southern Asia have been studied by Jena et al. (2014) reporting O<sub>3</sub> enhancements of 4-10 ppb (25-50%) in the Eastern region including Burma, 1-3 ppb (10-25%) in Central India and 1-7 ppb (4-10%) in the Indo-Gangetic region. Further, the O<sub>3</sub> enhancement was found to be about 2-6 ppb (8-20%) over the Bay of Bengal in March, which was attributed to transport from the Eastern region. Section 2 presents the model description, including physics and chemistry options, emission inputs and the observational data. Model evaluation focussing on the effects of different emission inventories on ozone is presented in section 3. The inter-comparison between the RADM2 and MOZART chemical mechanism is discussed in section 4. The sub-regional and South Asian domain evaluation and recommendations on model configuration are provided in section 5, followed by the summary and conclusions drawn from the study in section 6. The list of abbreviations and acronyms used in this paper are listed in Table 1.

## **2. Methodology**

### **2.1. WRF-Chem**

In this study we use the Weather Research and Forecasting model coupled with chemistry (WRF-Chem version 3.5.1), which is an online mesoscale model capable of simulating meteorological and chemical processes

simultaneously (Grell et al., 2005; Fast et al., 2006). The model domain (Fig. 1) is defined on a mercator projection and is centred at 22° N, 83° E with 274 and 352 grid points in the east-west and north-south directions, respectively, at the horizontal resolution of 12 km x 12 km. The land use data is incorporated from the US Geological Survey (USGS) based on 24 land use categories. The ERA-interim reanalysis dataset from ECMWF (<http://www.ecmwf.int/en/research/climate-reanalysis/browse-reanalysis-datasets>), archived at the horizontal resolution of about 0.7° and temporal resolution of 6 hours, is used to provide the initial and lateral boundary conditions for the meteorological calculations. All simulations in the study have been conducted for the period: 26<sup>th</sup> February – 31<sup>st</sup> May, 2013 at a time step of 72 s. The model output is stored every hour for analysis. The first three days of model output have been discarded as model spin up.

Radiative transfer in the model has been represented using the Rapid Radiative Transfer Model (RRTM) longwave scheme (Mlawer, 1997) and the Goddard shortwave scheme (Chou and Suarez, 1994). Surface physics is parameterized using the Unified Noah land surface model (Tewari et al., 2004) along with eta similarity option (Monin and Obukhov, 1954; Janjic, 1994, 1996), and the planetary boundary layer (PBL) is based on the Mellor-Yamada-Janjic (MYJ) scheme (Mellor and Yamada, 1982; Janjic, 2002). The cloud microphysics is represented by the Lin et al. scheme (Lin et. al., 1983), and cumulus convection is parameterized using the Grell 3D Ensemble Scheme (Grell, 1993; Grell and Devenyi, 2002). Four-dimensional data assimilation (FDDA) is incorporated for nudging to limit the drift in the model simulated meteorology from the ERA-interim reanalysis (Stauffer and Seaman, 1990; Liu et al. 2008). Horizontal winds are nudged at all vertical levels, whereas temperature and water vapour mixing ratios are nudged above the PBL (Stauffer et al. 1990, 1991). The nudging coefficients for temperature and horizontal winds are set as  $3 \times 10^{-4} \text{ s}^{-1}$  whereas it is set as  $10^{-5} \text{ s}^{-1}$  for water vapour mixing ratio (Otte, 2008).

This study utilizes two different chemical mechanisms, the Regional Acid Deposition Model - 2<sup>nd</sup> generation (RADM2) (Stockwell et al., 1990), and the Model for Ozone and Related Chemical Tracers-version 4 (MOZART-4) (Emmons et al., 2010). RADM2 chemistry includes 63 chemical species participating in 136 gas phase and 21 photolysis reactions. MOZART chemistry includes 81 chemical species participating in 159 gas phase and 38 photolysis reactions. Aerosols are represented using the Modal Aerosol Dynamics Model for Europe/ Secondary Organic Aerosol Model (MADE/SORGAM) (Ackermann et al., 1998; Schell et al., 2001) with RADM2 and Global Ozone Chemistry Aerosol Radiation and Transport (GOCART) (Chin et al., 2000) with MOZART. The photolysis rates are calculated using the Fast-J photolysis scheme (Wild et al., 2000) in RADM2 simulations and the Madronich FTUV scheme in the MOZART simulation. In WRF-Chem, the Madronich F-TUV photolysis scheme uses climatological O<sub>3</sub> and O<sub>2</sub> overhead columns. The treatment of dry deposition process also differs between RADM2 and MOZART owing to differences in Henry's Law coefficients and diffusion coefficients. The chemical initial and lateral boundary conditions are provided from 6 hourly fields from the Model for Ozone and Related Chemical Tracers (MOZART-4/GEOS5) (<http://www.acom.ucar.edu/wrf-chem/mozart.shtml>).

## 2.2. Emission inputs

This study utilizes three different inventories for the anthropogenic emissions: HTAP, INTEX-B and the SEAC4RS, which are briefly described here. The Hemispheric Transport of Air Pollution (HTAP) inventory (Janssens-Maenhout et al., 2015) for anthropogenic emissions ([http://edgar.jrc.ec.europa.eu/htap\\_v2/index.php?SECURE=\\_123](http://edgar.jrc.ec.europa.eu/htap_v2/index.php?SECURE=_123)) available for the year 2010 has been used. The HTAP inventory has been developed

by complementing various regional emissions with EDGAR data, in which Asian region including India is represented by the Model Intercomparison study for Asia (MICS-Asia) inventory, which is at a horizontal resolution of  $0.25^\circ \times 0.25^\circ$  (Carmichael et al., 2008). The resultant global inventory is re-gridded at the spatial resolution of  $0.1^\circ \times 0.1^\circ$  and temporal resolution of 1 month. HTAP includes emissions of CO, NO<sub>x</sub>, SO<sub>2</sub>, NM VOCs, PM, BC and OC from power, industry, residential, agriculture, ground transport and shipping sectors. The Intercontinental Chemical Transport Experiment-Phase B (INTEX-B) inventory (Zhang et al., 2009), developed to support the INTEX-B field campaign by the National Aeronautics and Space Administration (NASA) in spring 2006, is the second inventory used in this study. It provides total emissions for year 2006 at a horizontal resolution of  $0.5^\circ \times 0.5^\circ$ . The emission sectors include power generation, industry, residential and transportation. The Southeast Asia Composition, Cloud, Climate Coupling Regional Study (SEAC4RS) inventory (Lu and Streets, 2012), prepared for the NASA SEAC4RS field campaign, is the third inventory used in this study. It provides total emissions for the year 2012 at a spatial resolution of  $0.1^\circ \times 0.1^\circ$ . The SEAC4RS and INTEX-B did not cover regions in the north western part of the domain, and therefore we complemented this region (longitude  $< 75^\circ\text{E}$  and latitude  $> 25^\circ\text{N}$ ) by HTAP emission data. The emissions of CO, NM VOCs and NO<sub>x</sub> emissions among the three emission inventories, as included in the simulations, are shown in Fig. 2. Table 2 provides estimates of total emissions over different regions (as defined in Fig.1) from the three inventories. The total emissions over all regions show that HTAP has about 43% higher and SEAC4RS about 46% higher NO<sub>x</sub> emissions compared to the INTEX-B inventory. Also, HTAP has about 37% higher VOC emissions compared to SEAC4RS and about 49% higher compared to the INTEX-B inventory. Hence SEAC4RS, the most recent inventory of the three, has similar total NO<sub>x</sub> emissions as that in HTAP but the total VOC source is closer to INTEX-B, which is the oldest of the three inventories. Considering the non-linear dependence of O<sub>3</sub> formation on precursors, numerical experiments are necessary to assess the influence of such large differences among the inventories. The emissions from biomass burning are included using the Fire Inventory from NCAR (FINN) version 1.0 (Wiedinmyer et al., 2011). Model of Emissions of Gases and Aerosols from Nature (MEGAN) is used to include the biogenic emissions (Guenther et al., 2006) in the model.

The HTAP inventory is available at monthly temporal resolution while INTEX-B and SEAC4RS are available as annual averages; however, seasonal variability in anthropogenic emissions may not have a major effect in this study as we focus here on spring (pre-monsoon), for which monthly emissions are similar to the annual mean (seasonal factor close to unity) (Supplementary material - Fig. S1; also see Fig. 2b in Kumar et al., 2012b). Nevertheless, seasonal influence during spring is strongest for biomass-burning emissions, which have been accounted for. The emissions from all inventories were injected in the lowest model layer. The diurnal profiles of the anthropogenic emissions of ozone precursors, specific to South Asia are not available. A sensitivity simulation implementing the diurnal emission profile available for Europe (Mar et al., 2016 and references therein) showed a little impact on predicted noontime ozone over South Asia (Supplementary material – Fig S2).

### 2.3. Simulations

We have conducted 4 different numerical simulations as summarized in Table 3 and briefly described here. Three simulations correspond to three different emission inventories HTAP, INTEX-B and SEAC4RS for the anthropogenic emissions of ozone precursors, employing the RADM2 chemical mechanism. These simulations are named HTAP-RADM2, INTEX-RADM2 and S4RS-RADM2 respectively. The emissions of aerosols have been kept same (HTAP) among these three simulations and aerosol-radiation feedback has been switched off to

specifically identify the effects of emissions of O<sub>3</sub> precursors on modelled ozone. An additional simulation HTAP-MOZ has been conducted to investigate the sensitivity of ozone to the employed chemical mechanism (MOZART vs RADM2) by keeping the emissions fixed to HTAP.

#### 2.4. Observational dataset

Previous studies have shown that WRF-Chem accurately reproduces the synoptic scale meteorology over the Indian region, justifying its use for atmospheric chemical simulations (e. g. Kumar et al., 2012a). Further, nudging towards reanalysis data limits deviations in simulated meteorology (e. g. Kumar et al., 2012a; Ojha et al., 2016; Girach et al., 2017). Nevertheless, we include an evaluation of model simulated water vapour, temperature and wind speed against radiosonde observations (Supplementary material, Fig. S3). Vertical profiles of the monthly average (April) water vapour mixing ratio (g/Kg), temperature (°C) and horizontal wind speed (m/s) have been obtained from radiosonde data (available at <http://weather.uwyo.edu/upperair/sounding.html>) for evaluation of modelled meteorology over Delhi (in North India), Bhubaneshwar (in east India) and Ahmedabad (in west India). We find that model simulated meteorology is in good agreement (within 1-standard deviation variability) with the observations.

Surface ozone data is acquired from various studies and sources, as given in Table 4. In general, surface O<sub>3</sub> measurements over these stations have been conducted using the well-known technique of UV light absorption by ozone molecules at about 254 nm, making use of Beer-Lambert's Law. The accuracy of these measurements is reported to be about 5% (Kleinmann et al., 1994). The response time of such instruments is about 20 s and instruments have a lower detection limit of 1 ppbv (Ojha et al., 2012). Here we have used the hourly and monthly average data for the model evaluation. The details of instruments and calibrations at individual stations can be found in the references given in the Table 4. It is to be noted that most of the observations are conducted generally inside the campus of universities/ institutes, reasonably away from the direct roadside emissions / exhausts (see references provided in Table 4) and therefore not influenced by concentrated local pollution sources.

As simultaneous measurements at different stations are very sparse over South Asia, the model evaluation has often to be conducted using observations of the same season/month of a different year (e. g. Kumar et al., 2012b; Kumar et al., 2015; Ojha et al., 2016). However, to minimize the effect of temporal differences we preferentially used measurements of recent years i.e. the observations at the stations used in this study are of the period: 2009-2013. For four stations: Delhi (north India), Jabalpur (central India), Pune (west India) and Thumba (south India), the observations and simulations are for the same year (2013). Finally, we investigated the effects of temporal differences on the results and model biases presented here by conducting another simulation for a different year (2010) (Supplementary material, Fig. S4).

There is also a need to evaluate precursor mixing ratios over the region to further reduce uncertainties in modelled ozone over South Asia. However, very limited data is available for ozone precursors in India and adjacent countries (especially for non-methane volatile organic compounds; NMVOCs). We include an evaluation of modelled NO<sub>x</sub>, ethane and ethene mixing ratios against several recent observations in the supplementary material (see Table S1). More sensitive techniques (e.g. blue light converter for NO<sub>2</sub>) in future would provide better insights into model performance in reproducing NO<sub>x</sub> over India.

### 3. Effects of emission inventories

#### 3.1. Spatial distribution of Ozone

The spatial distribution of WRF-Chem simulated 24-h monthly average ozone during April is shown in Fig. 3a (upper panel) for the three different emission inventories (HTAP, INTEX, and SEAC4RS). Generally the months of March and May are marked with seasonal transition from winter to summer and summer to monsoon respectively. Hence, the month of April is chosen to represent the pre-monsoon season as it is not influenced by these seasonal transitions, and the observational data is available for a maximum number of stations during this month for the comparison. The 24-h average ozone mixing ratios are found to be 40-55 ppbv over most of the Indian subcontinent for all the three inventories. Model simulated ozone levels over the coastal regions are also similar (30-40 ppbv) among the three inventories. The highest ozone mixing ratios (55 ppbv and higher) predicted in the South Asian region are found over northern India and the Tibetan Plateau. The WRF-Chem simulated spatial distributions of average ozone shown here are in agreement with a previous evaluation study over South Asia (Kumar et al., 2012b). Further, it is found that qualitatively as well as quantitatively the HTAP, INTEX-B and SEAC4RS lead to very similar distributions of 24-h average ozone over most of the South Asian region. The 24h monthly average ozone from observations is superimposed on the model results in Fig. 3a for comparison. WRF-Chem simulated distributions of average O<sub>3</sub> are in general agreement with the observational data (Fig. 3a), except at a few stations near coasts (e. g. Kannur and Thumba) and in complex terrain (Pantnagar and Dibrugarh). In contrast to the distribution of 24-h average O<sub>3</sub>, the noontime (1130-1630 IST) O<sub>3</sub> mixing ratios over continental South Asia exhibit significant differences among the three emission inventories (Fig. 3b). HTAP clearly leads to higher noontime O<sub>3</sub> mixing ratios, the difference being up to 10 ppbv over the Indo-Gangetic plain (IGP), 20 ppbv over Central India, and 30 ppbv over Southern India, compared to INTEX-B and SEAC4RS. The mean bias (MB) (model-observation) for 24-h and noontime average ozone at individual stations is provided in the supplementary material - Table S2 and S3. A sensitivity simulation is conducted to reveal the influence of a different cumulus parameterization (Kain-Fritsch scheme) on our conclusions. The differences in the modelled surface ozone mixing ratios over most of the Indian domain are found to be within  $\pm 5\%$  (supplementary material; Figure S5). The relatively large differences over some of the Indian region indicate that the Kain-Fritsch scheme tends to predict higher surface ozone mixing ratios relative to the base run (incorporating Grell 3D Ensemble Scheme), which would only add up to biases in the original runs. Therefore our conclusions are not affected.

The net photochemical O<sub>3</sub> production rate (ppbv h<sup>-1</sup>) from sunrise to noontime (0630-1230 IST), when most of the photochemical build-up of ozone takes place leading to its peak noontime mixing ratio, has been calculated utilizing the chemical tendencies in WRF-Chem (Barth et al., 2012; Girach et al., 2017). A comparison of monthly average O<sub>3</sub> production rates among the three inventories is shown in Fig. 4. As seen also from the O<sub>3</sub> mixing ratios (Fig. 3b), the HTAP emissions result in faster O<sub>3</sub> production ( $\sim 9$  ppbv h<sup>-1</sup>) throughout the IGP region. The highest O<sub>3</sub> production rates for INTEX-B and SEAC4RS inventories are simulated only in the East Indian regions including the eastern parts of the IGP. It is noted that the rate of O<sub>3</sub> production is lower (4-8 ppbv h<sup>-1</sup>) over most of the south-western IGP for the INTEX-B and SEAC4RS inventories. Differences are also found over the southern Indian region with stronger ozone production in HTAP, followed by INTEX-B and SEAC4RS.

Figure 5 provides insight into the spatial distribution of O<sub>3</sub> production regimes estimated through the CH<sub>2</sub>O/NO<sub>y</sub> ratio (Geng et al., 2007; Kumar et al. 2012b) calculated during 0630 – 1230 IST, to help explain the differences in

modelled ozone mixing ratios among the three simulations. The metric  $\text{CH}_2\text{O}/\text{NO}_y$ , as described by Sillman (1995), is suggested to be a useful diagnostic to determine the ozone production regime. Sillman (1995) evaluated the correlation between  $\text{O}_3$ - $\text{NO}_x$ -VOC sensitivity predicted by photochemical model and  $\text{CH}_2\text{O}/\text{NO}_y$  ratio. The correlation has been derived combining results from serial computations with the model by varying the anthropogenic and biogenic emissions, and meteorology. The method has been successfully employed in investigating ozone distribution over the South Asia (Kumar et al., 2012b), East Asia (Geng et al., 2007; Tie et al., 2013), and Europe (Mar et al., 2016). Tie et al (2013) reported similarities between the results based on the  $\text{CH}_2\text{O}/\text{NO}_y$  ratio and those following another method described by Kleinmann et al. (2003) over Shanghai. A value of 0.28 for  $\text{CH}_2\text{O}/\text{NO}_y$  ratio is suggested to be the transitional value from VOC limited regime to  $\text{NO}_x$  limited regime. The spatial distribution of regimes in all simulations in the present study is largely consistent with the findings of Kumar et al. (2012b) although the latter performed the analysis for afternoon hours (1130 – 1430 IST). The S4RS-RADM2 simulation predicts the entire IGP to be VOC sensitive whereas in HTAP-RADM2 and INTEX-RADM2 simulations though the northwest IGP and eastern IGP are VOC sensitive, the central IGP is mostly  $\text{NO}_x$  limited. The coastal regions are also predicted to be VOC limited in all the three simulations. With the north-western IGP being VOC limited in all simulations, the noontime ozone mixing ratios are found to be higher in this region in HTAP-RADM2 simulation because of high NMVOC emissions in HTAP inventory as evident from figure 2 and table 2. Similar differences are also apparent in southern India.

Some of the ozone precursors ( $\text{NO}_x/\text{NO}_y$ , ethane and ethene) are also compared between model and recent measurements over few stations (Table S1). Significant differences are seen in model simulated  $\text{NO}_x$  mixing ratios among different emission inventories (e. g. 6.5-30.5 ppbv at Kanpur) over the urban stations in the IGP. Model typically overestimated  $\text{NO}_x$  mixing ratios at Delhi except in INTEX-RADM2 simulation, which showed an agreement with observations within 1-standard deviation. Total nitrogen oxides ( $\text{NO}_y$ ) showed relatively similar levels among different inventories (2.7-3.2 ppbv) at a high-altitude station (Nainital) in north India and were only slightly higher than observed mean ( $1.8 \pm 1.6$  ppbv). In contrast with the stations in northern India,  $\text{NO}_x$  levels over a rural station Udaipur in western India are underestimated by a factor of 4. On the other hand, modelled ethane mixing ratios are underpredicted by a factor of about 2 whereas modelled ethene mixing ratios agree relatively well with observed values at Nainital in INTEX-RADM2 and S4RS-RADM2 as compared to HTAP-RADM2. More in situ observations, especially of ozone precursors, may provide better insights into the performance of the numerical models and employed emission inventories over this region.

In summary, these results show similar 24-h average ozone distributions but large differences in the ozone build-up until noon. The net photochemical ozone production in the morning hours (0630-1230) is shown to be sensitive to the different inventories over this region, which is attributed to differences in total  $\text{NO}_x$  and/or NMVOC emissions. We therefore suggest that a focus on 24-h averages only would be insufficient to evaluate the ozone budget and implications for human health and crop yield. Next we compare the modeled diurnal ozone variations from three inventories with in situ measurements over 15 stations across the South Asia.

### 3.2. Diurnal variation

A comparison of WRF-Chem simulated diurnal ozone variability with recent in situ measurements over a network of 15 stations in the South Asian region is shown in Fig. 6. WRF-Chem is found to successfully reproduce the



characteristic diurnal ozone patterns observed over the urban (e.g. Mohali, Delhi, Kanpur, Ahmedabad, Bhubaneswar and Pune) and rural (e.g. Anantpur, Gadanki) stations, indicating strong ozone build-up from sunrise to noontime and the predominance of chemical titration (by NO) and deposition losses during the night. In general, WRF-Chem captures the daily amplitude of O<sub>3</sub> changes at relatively cleaner and high altitude stations, typically showing less pronounced diurnal variability, such as Nainital in the Himalayas, although with differences in timing when model and observations attain minimum ozone mixing ratios, thus leading to relatively low correlation coefficient (see later in the text). The diurnal variability in O<sub>3</sub> indicated by  $\Delta O_3$ , i.e. the difference between diurnal mean and hourly values, is further compared between the model and observations at all the stations (Supplementary material – Fig S6). This comparison intends to focus more on to evaluate the model's ability to reproduce different diurnal patterns over urban, rural and clean chemical environments and minimizing the representation of absolute ozone levels. It is seen that model successfully captures the observed variability in ozone at most of the sites in this region. However, a limitation is noticed in resolving well the stations in the vicinity of complex terrain (such as Jabalpur), attributed to the stronger spatial heterogeneity due to forests, hills and mountains within a small area (Sarkar et al., 2015).

To briefly evaluate the possible effects due to the difference in meteorological year between model and observations, we repeated the HTAP-RADM2 simulation for a different year (2010) as shown in the Supplementary material – Fig. S4. The effect of changing the meteorological year in the model simulation is generally small (mostly within  $\pm 3$  ppbv in 3 years), except at a few stations in the north (Nainital and Pantnagar) and east (Bhubaneswar). The effect is seen to vary from 4.8 ppbv to 6 ppbv (in 3 years) at these three stations. These differences are found to be associated with the inter-annual variations in the regional and transported biomass burning emissions, as seen from MODIS fire counts and MOZART/GEOS5 boundary conditions (not shown here).

The model ability to reproduce diurnal variations at all stations is summarised using a Taylor diagram (Taylor, 2001) in Figure 7. The statistics presented are normalised standard deviation (SD), normalised centred root mean squared difference (RMSD) and the correlation coefficient. The normalisation of both SD and RMSD is done using the standard deviation of the respective observational data. The point indicated as 'REF' represents the observational data against which the model results are evaluated. WRF-Chem simulations show reasonable agreement with observations showing correlation coefficients generally greater than 0.7 for most sites. The locations such as Nainital and Jabalpur for which *r* values are lower (0.3-0.7) are associated with unresolved complex terrain, as mentioned earlier. Note that the Taylor diagram has been used to present evaluation statistics for a general overview and inter-comparison i.e. how the model reproduces the diurnal variation at different stations, irrespective of the emission inventory.

#### **4. Effects of chemical mechanism (RADM2 vs MOZART)**

Choice of chemical mechanisms in the regional models can also be an important element in the prediction of ozone. Inclusion of additional chemical species along with insufficient information on region-specific speciation factors could induce uncertainties to the predicted ozone. Further, in order to reduce the computational costs most chemical mechanisms in the models make use of lumping approach to reduce the number of chemical reactions thus avoiding treatment of all chemical species (Zaveri et al., 1999; Sarkar et al., 2016). In addition, different reaction rate constants, photolysis and dry deposition schemes used in the mechanisms are some of the factors

leading to the uncertainties. A recent WRF-Chem evaluation over Europe showed better agreement with in situ measurements when the MOZART chemical mechanism was employed, compared to RADM2 (Mar et al., 2016). Following up on this, here we compare modelled ozone mixing ratios obtained with these two extensively used chemical mechanisms over South Asia: RADM2 (e. g. Michael et al., 2013; Ojha et al., 2016, Girach et al., 2017) and MOZART (e. g. Ghude et al., 2014; Ghude et al., 2016), keeping the same input emission inventory (HTAP). In the present study, the photolysis rates are calculated using the Fast-J photolysis scheme (Wild et al., 2000) in RADM2 simulations and the Madronich FTUV scheme in the MOZART simulation. In WRF-Chem, the Madronich F-TUV photolysis scheme uses climatological O<sub>3</sub> and O<sub>2</sub> overhead columns. The treatment of dry deposition process also differs between RADM2 and MOZART owing to differences in Henry's Law coefficients and diffusion coefficients. Thus, the following sensitivity analysis is aimed at exploring if the use of the more detailed chemical mechanism of MOZART could improve the model performance.

#### 4.1. Spatial distribution of surface O<sub>3</sub>

The WRF-Chem simulated spatial distributions of 24-h average and noontime average surface ozone are compared in Fig. 8. The monthly values of the 24-h and noontime ozone mixing ratios from measurements are also shown. Overall, the average ozone mixing ratios over South Asia are simulated to be higher with the MOZART chemical mechanism compared to RADM2, which is consistent with the results of Mar et al. (2016) for the European domain. The 24-h average ozone mixing ratios over India simulated with MOZART chemistry are found to be higher than those with RADM2 chemistry, especially over the eastern Indian region (~60 ppbv and more for MOZART compared to ~40-55 ppbv for RADM2). Average ozone levels over the coastal regions are found to be similar between the two mechanisms (30-40 ppbv). MOZART chemistry also predicts high 24-h average ozone mixing ratios (55 ppbv and higher) over the Tibetan Plateau region, similar to RADM2. A striking difference between the two chemical mechanisms is found over the marine regions adjacent to South Asia (Bay of Bengal and northern Indian Ocean), with MOZART predicting significantly higher 24-h average ozone levels (35-50 ppbv) compared to the RADM2 (25-40 ppbv). A comparison of noontime average ozone distributions between the two chemical mechanism shows that MOZART predicts higher ozone concentrations than RADM2 over most of the Indian region by about 5-20 ppbv, except over western India. The differences are up to 20 ppbv and more over the Southern Indian region, highlighting the impacts of chemical mechanisms on modelled ozone in this region. The mean bias (MB) values (model-observation) for 24-h and noontime average ozone at individual stations is provided in the supplementary material - Table S2 and S3.

Figure 9a shows a comparison of the monthly average chemical O<sub>3</sub> tendency (ppbv h<sup>-1</sup>) from 0630 to 1230 IST. In contrast with average O<sub>3</sub> mixing ratios, which were found to be higher in HTAP-MOZ, the net O<sub>3</sub> production rates at the surface are higher in HTAP-RADM2 over most of the domain, especially in the IGP and central India. The net O<sub>3</sub> production rates at the surface with HTAP-RADM2 are found to be 6 to 9 ppbv h<sup>-1</sup> and more over the IGP, whereas these values are generally lower in HTAP-MOZ (4-8 ppbv h<sup>-1</sup>), except in the north-eastern IGP (>9 ppbv h<sup>-1</sup>). Fig. 9b shows the sum of the chemical tendency and vertical mixing tendency at the surface for the HTAP-RADM2 and HTAP-MOZ. Analysis of the vertical mixing tendency revealed that higher surface ozone mixing ratios in the MOZART simulation are due to mixing with ozone rich air from aloft. In the HTAP-RADM2 simulation, vertical mixing dilutes the effect of strong chemical surface ozone production. Further analysis of vertical distributions of chemical O<sub>3</sub> tendencies reveals stronger photochemical production of ozone aloft with MOZART compared to RADM2 (Supplementary material-Fig. S7). This leads to higher ozone mixing ratios aloft

in MOZART simulations. A sensitivity simulation is conducted using a different PBL parameterization (Yonsei University Scheme) to examine its influence on our conclusions. Comparison of monthly average (in April) planetary boundary layer heights between the two PBL schemes revealed that the differences are mostly within  $\pm 150$  m with Yonsei scheme generally resulting in higher PBL heights over India (Fig. S9). Nevertheless, the chemical tendencies combined with vertical mixing tendencies of surface  $O_3$  are found to be nearly similar with Yonsei scheme (Fig. S10) as in the base runs using the MYJ scheme (Fig. 9b) with MOZART still producing higher ozone aloft (not shown) as in the original runs. Thus changing the PBL scheme still results in production of more ozone aloft in MOZART, which is getting mixed with near surface air, which corroborates that our conclusions are not affected.

Mar et al. (2016) showed that RADM2 exhibits greater VOC sensitivity than MOZART (i.e., producing higher changes in ozone given a perturbation in VOC emissions) under noontime summer conditions over Europe. This is consistent with our findings as well, that the net surface photochemical ozone production is greater for HTAP-RADM2 than for HTAP-MOZART, given the high VOC emissions in the HTAP inventory. At the surface, the MOZART mechanism predicts larger areas of VOC-sensitivity (as diagnosed by the  $CH_2O/NO_y$  indicator, Figure 10) and lower net photochemical ozone production than RADM2. With increasing altitude, both the HTAP-RADM2 and HTAP-MOZART simulations show a general increase of  $CH_2O/NO_y$  over India, i.e. the chemistry tends to exhibit increased  $NO_x$  sensitivity with increasing height (Supplementary material-Figure S11). At model levels above the surface, HTAP-MOZART shows greater net photochemical production of ozone than HTAP-RADM2 (Supplementary material-Figure S7), which is what Mar et al. (2016) have also reported for the surface  $O_3$  over Europe. When these effects are combined, mixing leads to higher surface ozone mixing ratios for HTAP-MOZART than for HTAP-RADM2. A sensitivity simulation using a different photolysis scheme (Madronich TUV photolysis scheme) with HTAP-RADM2 setup revealed similar surface ozone mixing ratios and chemical tendencies at various model levels with small differences ( $<5\%$ ) over most of the Indian region (not shown). So our results would be similar if we use Madronich TUV scheme instead of Fast-J scheme with RADM2. Further, Mar et al. (2016) used Madronich TUV scheme with RADM2 and Madronich F-TUV scheme with MOZART chemical mechanism and reported that the two different Madronich photolysis schemes had only a small contribution to the differences in the predicted ozone by two chemical mechanisms. The major difference between the two chemical mechanisms was due to differences in inorganic reaction rates (Mar et al, 2016). Hence we conclude that in our study too, the differences over Indian region are primarily due to the choice of the chemical mechanisms irrespective of photolysis scheme used. Also note that the aerosol radiation feedback is turned off, so that the calculated differences mainly result from the representation of gas phase chemistry rather than of aerosols between MOZART and RADM2. Our analysis also shows the importance of chemical regime in understanding differences between the chemical mechanisms, and highlights the significant effects of the employed chemical mechanism on modelled ozone over South Asia.

#### 4.2. Diurnal variation

Figure 11 shows a comparison of WRF-Chem simulated ozone variations on diurnal timescales with recent in situ measurements over a network of stations across the South Asia for the two chemical mechanisms (MOZART and RADM2); again with the same emission inventory (HTAP). Qualitatively, both simulations produce very similar diurnal patterns (also see Supplementary material, Fig. S12), however, the absolute  $O_3$  mixing ratios are found to

differ significantly (Figure 11) between the two chemical mechanisms. Noontime ozone mixing ratios predicted by MOZART are either significantly higher (at 9 out of 15 stations) or nearly similar (at 6 stations). MOZART-predicted O<sub>3</sub> at Dibrugarh, Kanpur, Jabalpur, Bhubaneswar, Gadanki and Thumba was found to be higher by ~12 ppbv, 5 ppbv, 8 ppbv, 10 ppbv, 11 ppbv and 12 ppbv, respectively, compared to RADM2 (Supplementary material, Table S3). Over several urban and rural stations in India (e.g. Delhi, Ahmedabad, Pune, Kannur and Thumba) MOZART is found to titrate ozone more strongly during the night while resulting in higher or similar ozone levels around noon. The contrasting comparison between noon and night time found at these sites suggests that evaluation limited to 24 h averages would not be sufficient, and that model performance on a diurnal time scale should be considered to assess the photochemical build-up of O<sub>3</sub>.

The model performance of two chemical mechanisms in reproducing diurnal variation at all stations is summarised using a Taylor diagram in Fig. 12. Both chemical mechanisms show reasonably good agreement ( $r > 0.7$ ) at most of the sites, except one station associated with highly complex terrain (Nainital). On the Taylor diagram, most of the HTAP-RADM2 results are found to be closer to the 'REF', as compared to HTAP-MOZ results, suggesting that the RADM2 chemical mechanism is better suited to simulate diurnal variation of ozone over this region.

## 5. Overall evaluation

In this section, we present a sub-regional evaluation of all simulations by subdividing the domain into five geographical areas, i.e. North, South, East, West and central India, as shown in Fig. 1. The temporal correlation coefficients of diurnally varying O<sub>3</sub>, spatially averaged over each of the five different sub-regions, are found to be reasonably high, generally exceeding 0.7 (Table 5). The  $r$  values for individual sub-regions are found to be similar among the four simulations. For example, over north India the  $r$  values vary from 0.86 to 0.90. The model performance differs among several sub-regions, with correlations being lower for central India ( $r = 0.67-0.75$ ). Since the latter is based on only one station associated with complex terrain (Jabalpur), we suggest that observations over additional stations should be conducted to evaluate the model performance in the central Indian region. The mean bias values around noontime are provided in supplementary material (Table S5). These results show that the performance of emission inventories is regionally different, and that these biases should be considered in utilizing model for assessment of air quality and impacts on human health and crop yield.

We finally evaluate the different simulations in the context of the entire south Asian region. Figure 13 shows a comparison of model results and measurements with diurnal box/whisker plots, combining all stations for the four different simulations. It is clearly seen that HTAP-MOZ yields highest noontime surface ozone mixing ratios among all simulations followed by HTAP-RADM2. These results further suggest that assessment of the tropospheric ozone budget as well as implications for public health and crop loss are associated with considerable uncertainty, and biases need to be considered. A recent study (Ghude et al., 2016) utilizing MOZART chemistry, for example, subtracted 15 ppbv from the WRF-Chem simulated ozone mixing ratios before deriving premature mortalities over the Indian region. The results of present study are summarized in the form of a polar plot (Fig. 14) showing the monthly mean diurnal variation from all runs for the entire south Asian domain. The noontime normalized mean bias values with respect to observed values are ~9.7% (S4RS-RADM2), ~11.5% (INTEX-RADM2), ~20.9% (HTAP-RADM2) and ~34.2% (HTAP-MOZ). It is to be noted that comparison of absolute ozone levels from model with observations has a limitation due to non-consideration of aerosol impacts and the

resolution at which the model results are obtained; nevertheless, it provides an estimate about the uncertainties in model predictions of ozone using different emission inventories. It is interesting to note that the SEAC4RS inventory (representative of year 2012) yields quite similar domain wide average bias value as the INTEX-B inventory (representative of year 2006).

## 6. Summary and conclusions

In this paper, we compare the WRF-Chem simulated surface ozone over South Asia during the pre-monsoon season by employing three different inventories (EDGAR-HTAP, INTEX-B, and SEAC4RS) for anthropogenic emissions with the RADM2 chemical mechanism. WRF-Chem simulated ozone distributions showed highest ozone mixing ratios (~55 ppbv and higher) over northern India and the Tibetan Plateau. In general, modelled average ozone distributions from different inventories are found to be in agreement with previous studies over this region. Evaluation on diurnal time scales demonstrates the ability of the model to reproduce observed O<sub>3</sub> patterns at urban and rural stations, showing strong noontime ozone build-up and chemical titration and deposition loss during the night-time. WRF-Chem also captures the smaller diurnal amplitudes observed over high altitude, relatively pristine stations. However, model showed limitations in capturing ozone mixing ratios in the vicinity of the complex terrain, indicating that even a relatively high horizontal resolution of 12 km x 12 km could not fully resolve the topography induced effects.

Overall WRF-Chem simulations show reasonable agreement with observations, with correlation coefficients generally higher than 0.7 for most of the sites. It is found that the HTAP, INTEX-B and SEAC4RS inventories lead to very similar distributions of 24-h average ozone over this region. This is corroborated by the quantitative similarity in simulated surface ozone among the three simulations, for both 24h and noontime (1130-1630 IST) averages at all grids in the domain (supplementary material, table S6). However, noontime (1130-1630 IST) O<sub>3</sub> mixing ratios over continental South Asia differ significantly among the three inventories. This can also be seen in the quantitative assessment of similarity (Table S6), where the variance of the residual shows that the scatter is greater for the noontime averages than for the 24 h averages. HTAP inventory generally leads to noontime O<sub>3</sub> mixing ratios higher by 10 ppbv over the Indo-Gangetic plain (IGP), 20 ppbv over Central India, and 30 ppbv over Southern India, compared to the INTEX-B and SEAC4RS inventories. A comparison of monthly average O<sub>3</sub> net production rate during 0630-1230 IST among the three inventories shows that the HTAP emissions result in faster O<sub>3</sub> production (~9 ppbv h<sup>-1</sup>) throughout the IGP region compared to the other two inventories. Differences are also found over the southern Indian region with stronger ozone production in HTAP, followed by INTEX-B and SEAC4RS. The results show similar 24-h average ozone distributions, but large differences in noontime ozone build up, pointing to the uncertainties in emission inventories over this region.

We further investigated the sensitivity of modelled ozone to two extensively used chemical mechanisms, RADM2 and MOZART, and maintaining the HTAP emissions. Noontime average surface ozone distributions predicted by MOZART show significant enhancements (10-15 ppbv) with respect to RADM2 over most of the Indian region, except over western India. MOZART predicts higher ozone concentrations than RADM2 by up to 20 ppbv and more over the South Indian region. Monthly average ozone mixing ratios are predicted to be higher by the MOZART chemical mechanism compared to RADM2, as was also found over Europe (Mar et al., 2016). The differences in ozone production between the MOZART and RADM2 chemical mechanisms are mainly attributed to the additional chemical species and reactions, differences in the rate constants for several inorganic reactions,

and photolysis schemes used. The difference in photolysis rates for  $\text{O}^1\text{D}$  and  $\text{NO}_2$  can be seen in supplementary material (Figure S13) for a surface point in the centre of the domain. A comparison of the monthly average chemical  $\text{O}_3$  tendency ( $\text{ppbv h}^{-1}$ ) during 0630-1230 IST shows that in contrast with average  $\text{O}_3$  mixing ratios, which were found to be higher in MOZART, the net  $\text{O}_3$  production rates at the surface are higher with RADM2 chemistry, especially over the IGP and central India. The net  $\text{O}_3$  production rates at the surface with RADM2 are found to be 6 to 9  $\text{ppbv h}^{-1}$ , and higher over the IGP, whereas these rates are generally lower with MOZART (4-8  $\text{ppbv h}^{-1}$ ), except in the northeastern IGP ( $>9 \text{ ppbv h}^{-1}$ ). Analysis of the vertical mixing tendency revealed that higher surface ozone mixing ratios in the MOZART simulation are due to mixing with ozone rich air from aloft. Analysis of vertical distributions of chemical  $\text{O}_3$  tendencies reveals stronger photochemical production of ozone aloft with MOZART compared to RADM2. Our analysis highlights the significant effects of the employed chemical mechanism on model predicted ozone over South Asia.

Qualitatively, RADM2 and MOZART simulations predict similar diurnal patterns. However, over several urban and rural stations in India MOZART is found to titrate ozone relatively strongly during the night, while producing higher or similar ozone levels during noontime compared to RADM2. The contrasting evaluation results between day- (noon) and night-time could counterbalance in evaluation studies limited to 24 h averages, possibly showing better agreement and therefore it is pertinent to consider the diurnally resolved model performance.

Model results averaged over all observation sites encompassing the South Asian region revealed that HTAP-MOZ predicts highest noontime ozone mixing ratios followed by HTAP-RADM2. The noontime normalized mean bias compared to observations is lowest for the SEAC4RS inventory with the RADM2 chemical mechanism ( $\sim 9.7\%$ ), followed by INTEX-B with RADM2 ( $\sim 11.5\%$ ), HTAP with RADM2 ( $\sim 20.9\%$ ), and HTAP with MOZART ( $\sim 34.2\%$ ). These results further suggest that the assessment of the tropospheric ozone budget and consequently its implications on public health and agricultural output should be carried out cautiously by considering the large uncertainties associated with use of emission inventories and chemical mechanism incorporated. As we report considerable differences in the noontime ozone levels among different inventories, further work is needed to account for aerosol feedback, and evaluation of ozone precursors to identify best suited emission inventory for this region. Modelled levels of ozone precursors showed significant differences among simulations employing the three emission inventories with an overestimation of  $\text{NO}_x$  levels at urban stations in the IGP. Evaluation of model simulated levels of ozone precursors over a network of observations is highly desirable, as conducted for ozone in this study. It is interesting to note that the SEAC4RS inventory (representative of 2012) yields results comparable to the INTEX-B inventory (for 2006), even though the SEAC4RS inventory has about 46% higher  $\text{NO}_x$ , 9% higher NMVOC and 15% lower CO emissions compared to INTEX-B.

Brown carbon aerosol can effectively absorb solar radiation (Alexander et al., 2008; Hecobian et al., 2010; Kirchstetter and Thatcher, 2012; Kirchstetter et al., 2004; Yang et al., 2009; Jo et al., 2016) leading to a reduction in  $\text{NO}_2$  photolysis rates and subsequently in surface ozone mixing ratios (Jo et al., 2016). Jo et al. (2016) reported that on an annual average basis, changes in surface ozone mixing ratios related to brown carbon aerosol absorption over South Asia are  $<5\%$ . Further studies should be taken up in the future to investigate the impact of aerosols on surface ozone, also with regional models like WRF-Chem. The current and other modelling efforts, constrained by limited measurement data, stress the need for more comprehensive observations, e.g. in a network of stations, and making the data available through projects such as TOAR (<http://toar-data.fz-juelich.de/>). Our study highlights the

need to also evaluate O<sub>3</sub> precursors, similar to that conducted here for ozone, to further reduce uncertainties in modelled ozone over South Asia for the better assessment of implications of surface ozone on public health and crop yield. In order to make better model predictions at further higher resolution (than 12 km), development of finer resolution inventories than the ones used in the current study is also required over the region. So we also recommend preparing high-resolution regional inventories for the anthropogenic emissions of O<sub>3</sub> precursors over South Asia, also accounting for year-to-year changes.

**Data availability:** The model output from all the numerical simulations is available at the MPG supercomputer HYDRA (<http://www.mpcdf.mpg.de/services/computing/hydra>) and would be provided by contacting the corresponding authors. The observed values shown for comparison are from previous papers with complete list of references provided in the Table 4. New observations for Delhi and Pune stations are available from the SAFAR program (<http://safar.tropmet.res.in/>).

## Acknowledgement

A. Sharma acknowledges the fellowship from the Max Planck Institute for Chemistry to carry out this study. S. S. Gunthe acknowledges the support from DST-Max Planck partner group at IIT Madras and Ministry of Earth Sciences (MoES), Govt. of India. Model simulations have been performed on the MPG supercomputer HYDRA (<http://www.mpcdf.mpg.de/services/computing/hydra>). Initial and boundary conditions data for meteorological fields were obtained from ECMWF website (<http://www.ecmwf.int/en/research/climate-reanalysis/era-interim>). The HTAP v2 anthropogenic emissions were obtained from [http://edgar.jrc.ec.europa.eu/htap\\_v2/index.php?SECURE=123](http://edgar.jrc.ec.europa.eu/htap_v2/index.php?SECURE=123). Authors are grateful to Yafang Cheng (MPI-C) for providing SEAC4RS emission. The INTEX-B anthropogenic emissions were obtained from [http://bio.cgrer.uiowa.edu/EMISSION\\_DATA\\_new/data/intex-b\\_emissions/](http://bio.cgrer.uiowa.edu/EMISSION_DATA_new/data/intex-b_emissions/). MOZART-4/ GEOS5 output used as initial and boundary conditions for chemical fields is acknowledged. The pre-processors and inputs for biogenic and biomass-burning emissions were obtained from NCAR Atmospheric Chemistry website (<http://www.acd.ucar.edu/wrf-chem/>). Radiosonde data of water vapour mixing ratio, temperature and wind speed were obtained from University of Wyoming website (<http://weather.uwyo.edu/upperair/sounding.html>). Authors are also thankful for the usage of HPC supercluster and to the staff at P. G. Senapathy Computer Center at IIT Madras. Constructive comments and suggestions from two anonymous reviewers, and the handling editor William Bloss are gratefully acknowledged.

## References

- Ackermann, I. J., Hass, H., Memmesheimer, M., Ebel, A., Binkowski, F. S., and Shankar, U.: Modal aerosol dynamics model for Europe: development and first applications, *Atmos. Environ.*, 32, 2981–2999, doi:10.1016/S1352-2310(98)00006-5, 1998.
- Ainsworth, E. A., Yendrek, C. R., Sitch, S., Collins, W. J., and Emberson, L. D.: The effects of tropospheric ozone on net primary productivity and implications for climate change, *Ann. Rev. Plant Biol.*, 63, 637–661, 2012.
- Akimoto, H.: Global air quality and pollution, *Science*, 302, 1716–1719, doi:10.1126/science.1092666, 2003.
- Alexander, D. T. L., Crozier, P. A., and Anderson, J. R.: Brown carbon spheres in East Asian outflow and their optical properties, *Science*, 321, 833–836, doi:10.1126/science.1155296, 2008.

592 Amnuaylojaroen, T., Barth, M. C., Emmons, L. K., Carmichael, G. R., Kreasuwun, J., Prasitwattanaseree, S., and  
 593 Chantara, S.: Effect of different emission inventories on modeled ozone and carbon monoxide in Southeast Asia,  
 594 *Atmos. Chem. Phys.*, 14, 12983-13012, doi:10.5194/acp-14-12983-2014, 2014.

595 Anenberg, S. C., Horowitz, L. W., Tong, D. Q., and West, J. J.: An estimate of the global burden of anthropogenic  
 596 ozone and fine particulate matter on premature human mortality using atmospheric modelling, *Environmental*  
 597 *Health Perspectives*, 118, 1189–1195, 2010.

598 Ansari, T. U., Ojha, N., Chandrasekar, R., Balaji, C., Singh, N. and Gunthe, S. S.: Competing impact of  
 599 anthropogenic emissions and meteorology on the distribution of trace gases over Indian region, *J. Atmos. Chem.*,  
 600 doi:10.1007/s10874-016-9331-y, 2016.

601 Atkinson, R.: Atmospheric chemistry of VOCs and NO<sub>x</sub>, *Atmos. Environ.*, 34, 2063–2101, doi:10.1016/S1352-  
 602 2310(99)00460-4, 2000.

603 Barth, M. C., Lee, J., Hodzic, A., Pfister, G., Skamarock, W. C., Worden, J., Wong, J., and Noone, D.:  
 604 Thunderstorms and upper troposphere chemistry during the early stages of the 2006 North American Monsoon,  
 605 *Atmos. Chem. Phys.*, 12, 11003-11026, doi:10.5194/acp-12-11003-2012, 2012.

606 Beig, G., Gunthe, S., and Jadhav, D. B.: Simultaneous measurements of ozone and its precursors on a diurnal scale  
 607 at a semi urban site in India, *JOURNAL OF ATMOSPHERIC CHEMISTRY*, 57, 239-253, doi: 10.1007/s10874-  
 608 007-9068-8, 2007.

609 Bell, M. L., McDermott, A., Zeger, S. L., Samet, J. M., and Dominici, F.: Ozone and short term mortality in 95 US  
 610 urban communities, 1987-2000, *JAMA The Journal of the American Medical Association*, 292, 2372-2378, 2004.

611 Bhuyan, P.K., Bharali, C., Pathak, B., and Kalita, G.: The role of precursor gases and meteorology on temporal  
 612 evolution of O<sub>3</sub> at a tropical location in northeast India, *Environmental Science and Pollution Research*, 21, 6696–  
 613 6713, 2014.

614 Carmichael, G. R., Sakurai, T., Streets, D., Hozumi, Y., Ueda, H., Park, S. U., Funge, C., Han, Z., Kajino, M.,  
 615 Engardt, M., Bennet, C., Hayami, H., Sartelet, K., Holloway, T., Wang, Z., Kannari, A., Fu, J., Matsuda, K.,  
 616 Thongboonchoo, N., and Amann, M.: MICS-Asia II: the model intercomparison study for Asia Phase II  
 617 methodology and overview of findings, *Atmos. Environ.*, 42, 3468–3490, doi:10.1016/j.atmosenv.2007.04.007,  
 618 2008.

619 Chin, M., Rood, R. B., Lin, S. -J., Muller, J. F., and Thomson, A. M.: Atmospheric sulfur cycle in the global  
 620 model GOCART: Model description and global properties, *J. Geophys. Res.*, 105, 24,671-24,687, 2000.

621 Chou, M. -D., and Suarez, M. J.: An efficient thermal infrared radiation parameterization for use in general  
 622 circulation models, NASA Technical Memorandum 104606, 3, 85pp, 1994.

623 Cox, R. A., Eggleton, A. E. J., Derwent, R. G., Lovelock, J. E., and Pack, D. H.: Long-range transport of  
 624 photochemical ozone in north-western Europe, *Nature*, 255, 118 – 121, doi:10.1038/255118a0, 1975.



Crutzen, P. J.: Photochemical reactions initiated by and influencing ozone in unpolluted tropospheric air, *Tellus*, 26, 47–57, 1974.

David, L. M., and Nair, P. R.: Diurnal and seasonal variability of surface ozone and NO<sub>x</sub> at a tropical coastal site: association with mesoscale and synoptic meteorological conditions, *Journal of Geophysical Research* 116, D10303. <http://dx.doi.org/10.1029/2010JD015076>, 2011.

Dumka, U. C., Krishna Moorthy, K., Kumar, R., Hegde, P., Sagar, R., Pant, P., Singh, N., and Suresh Babu, S.: Characteristics of aerosol black carbon mass concentration over a high altitude location in the central Himalayas from multi-year measurements, *Atmos. Res.*, 96, 510–521, 2010.

Emberson, L. D., Buker, P., Ashmore, M., Mills, G., Jackson, L., Agrawal, M., Atikuzzaman, M., Cinderby, S., Engardt, M., Jamir, C., Kobayashi, K., Oanh, N., Quadir, Q., and Wahid, A.: A comparison of North -American and Asian exposure-response data for ozone effects on crop yields, *Atmos. Environ.*, 43, 1945–1953, 2009.

Emmons, L. K., Walters, S., Hess, P. G., Lamarque, J.-F., Pfister, G. G., Fillmore, D., Granier, C., Guenther, A., Kinnison, D., Laepple, T., Orlando, J., Tie, X., Tyndall, G., Wiedinmyer, C., Baughcum, S. L., and Kloster, S.: Description and evaluation of the Model for Ozone and Related chemical Tracers, version 4 (MOZART-4), *Geosci. Model Dev.*, 3, 43–67, 20 doi:10.5194/gmd-3-43-2010, 2010.

Fast, J. D., Gustafson Jr., W. I., Easter, R. C., Zaveri, R. A., Barnard, J. C., Chapman, E. G., Grell, G. A. and Peckham, S. E.: Evolution of ozone, particulates, and aerosol direct radiative forcing in the vicinity of Houston using a fully-coupled meteorology-chemistry aerosol model, *Journal of Geophysical Research*, 111, D21305, 2006.

Gaur, A., Tripathi, S. N., Kanawade, V. P., Tare, V., and Shukla, S. P.: Four-year measurements of trace gases (SO<sub>2</sub>, NO<sub>x</sub>, CO, and O<sub>3</sub>) at an urban location, Kanpur, in Northern India, *J. Atmos. Chem.*, 71, 283–301, 2014.

Geng, F., Zhao, C., Tang, X., Lu, G., and Tie, X.: Analysis of ozone and VOCs measured in Shanghai: A case study, *Atmos. Environ.*, 41, 989–1001, 2007.

Ghude, S. D., Jena, C., Chate, D. M., Beig, G., Pfister, G. G., Kumar, R., and Ramanathan, V.: Reduction in India's crop yield due to ozone, *Geophys. Res. Lett.*, 41, 51971, doi:10.1002/2014GL060930, 2014.

Ghude, S. D., Chate, D. M., Jena, C., Beig, G., Kumar, R., Barth, M. C., Pfister, G. G., Fadnavis, S. and Pithani, P.: Premature mortality in India due to PM<sub>2.5</sub> and ozone exposure, *Geophysical Research Letters*, 43, 4650 – 4658, 2016.

Girach, I. A., Ojha, N., Nair, P. R., Pozzer, A., Tiwari, Y. K., Kumar, K. R., and Lelieveld, J.: Variations in O<sub>3</sub>, CO, and CH<sub>4</sub> over the Bay of Bengal during the summer monsoon season: shipborne measurements and model simulations, *Atmos. Chem. Phys.*, 17, 257–275, doi:10.5194/acp-17-257-2017, 2017.

Grell, G.: Prognostic evaluation of assumptions used by cumulus parameterizations, *Monthly Weather Review*, 121, 764–787, 1993.

658 Grell, G., and Devenyi, D.: A generalized approach to parameterizing convection combining ensemble and data  
659 assimilation techniques, *Geophys. Res. Lett.*, 29(14), 38–31, 2002.

660 Grell, G. A., Peckham, S. E., McKeen, S., Schmitz, R., Frost, G., Skamarock, W. C. and Eder, B.: Fully coupled  
661 ‘online’ chemistry within the WRF model, *Atmospheric Environment*, 39, 6957–6975, 2005.

662 Gupta, M. and Mohan, M.: Validation of WRF/Chem model and sensitivity of chemical mechanisms to ozone  
663 simulation over megacity Delhi, *Atmospheric Environment*, Volume 122, p. 220–229, 2015.

664 Guenther, A., Karl, T., Harley, P., Wiedinmyer, C., Palmer, P. I., and Geron, C.: Estimates of global terrestrial  
665 isoprene emissions using MEGAN (Model of Emissions of Gases and Aerosols from Nature), *Atmos. Chem.*  
666 *Phys.*, 6, 3181–3210, doi:10.5194/acp-6-3181-2006, 2006.

667 Gurjar, B. R., Ravindra, K., and Nagpure, A.S.: Air pollution trends over Indian megacities and their local-to-  
668 global implications, *Atmospheric Environment*, Volume 142, Pages 475–495,  
669 <http://dx.doi.org/10.1016/j.atmosenv.2016.06.030>, 2016.

670 Hecobian, A., Zhang, X., Zheng, M., Frank, N., Edgerton, E. S., and Weber, R. J.: Water-Soluble Organic Aerosol  
671 material and the light-absorption characteristics of aqueous extracts measured over the Southeastern United States,  
672 *Atmos. Chem. Phys.*, 10, 5965–5977, doi:10.5194/acp-10-5965-2010, 2010.

673 Jain, S. L., Arya, B. C., Kumar, A., Ghude, S. D., and Kulkarni, P. S.: Observational study of surface ozone at  
674 New Delhi, India, *Int. J. Remote Sens.*, 26, 3515–3524, 2005.

675 Janjic, Z. I.: The step-mountain eta coordinate model: further developments of the convection, viscous sublayer  
676 and turbulence closure schemes, *Monthly Weather Review* 122, 927–945, 1994.

677 Janjic, Z. I.: The surface layer in the NCEP Eta Model, Eleventh Conference on Numerical Weather Prediction,  
678 Norfolk, VA, 19–23 August; American Meteorological Society, Boston, MA, 354–355, 1996.

679 Janjic, Z. I.: Nonsingular Implementation of the Mellor–Yamada Level 2.5 Scheme in the NCEP Meso model,  
680 NCEP Office Note, No. 437, 61 pp, 2002.

681 Janssens-Maenhout, G., Crippa, M., Guizzardi, D., Dentener, F., Muntean, M., Pouliot, G., Keating, T., Zhang, Q.,  
682 Kurokawa, J., Wankmüller, R., Denier van der Gon, H., Kuenen, J. J. P., Klimont, Z., Frost, G., Darras, S., Koffi,  
683 B., and Li, M.: HTAP\_v2.2: a mosaic of regional and global emission grid maps for 2008 and 2010 to study  
684 hemispheric transport of air pollution, *Atmos. Chem. Phys.*, 15, 11411–11432, [http://dx.doi.org/10.5194/acp-15-](http://dx.doi.org/10.5194/acp-15-11411-2015)  
685 11411-2015, 2015.

686 Jena, C., Ghude, S. D., Pfister, G. G., Chate, D. M., Kumar, R., Beig, G., Surendran, D., Fadnavis, S., and Lal, D.  
687 M.: Influence of springtime biomass burning emissions in South Asia on regional ozone: A model based case  
688 study, *Atmos. Environ.*, 100, 37–47, doi:10.1016/j.atmosenv.2014.10.027, 2014.

689 Jena, C., Ghude, S. D., Beig, G., Chate, D. M., Kumar, R., Pfister, G. G., Lal, D. M., Surendran, D. E., Fadnavis,  
690 S., and van der, A. R. J.: Inter-comparison of different NO<sub>x</sub> emission inventories and associated variation in  
691 simulated surface ozone in Indian region, *Atmos. Environ.*, 117:61–73, 2015.

692 Jerrett, M., Burnett, R. T., Pope, C. A., III, Ito, K., Thurston, G., Krewski, D., et al.: Long-term ozone exposure  
 693 and mortality, *The New England Journal of Medicine*, 360, 1085–1095, 2009.

694 Jo, D. S., Park, R. J., Lee, S., Kim, S.-W., and Zhang, X.: A global simulation of brown carbon: implications for  
 695 photochemistry and direct radiative effect, *Atmos. Chem. Phys.*, 16, 3413–3432, doi:10.5194/acp-16-3413-2016,  
 696 2016.

697 Kirchstetter, T. W., Novakov, T., and Hobbs, P. V.: Evidence that the spectral dependence of light absorption by  
 698 aerosols is affected by organic carbon, *J. Geophys. Res.*, 109, D21208, doi:10.1029/2004JD004999, 2004.

699 Kirchstetter, T. W. and Thatcher, T. L.: Contribution of organic carbon to wood smoke particulate matter  
 700 absorption of solar radiation, *Atmos. Chem. Phys.*, 12, 6067–6072, doi:10.5194/acp-12-6067-2012, 2012.

701 Kleinman, L., Lee, Y. -N., Springston, S. R., Nunnermacker, L., Zhou, X., Brown, R., Hallock, K., Klotz, P.,  
 702 Leahy, D., Lee, J. H., and Newman, L.: Ozone formation at a rural site in the southeastern United States, *J.*  
 703 *Geophys. Res.-Atmos.*, 99, 3469–3482, doi:10.1029/93JD02991, 1994.

704 Kleinman L. I., Daum, P. H., Lee, Y.-N., Nunnermacker, L. J., Springston, S. R., Weinstein-Lloyd, J., Hyde, P.,  
 705 Doskey, P., Rudolph, J., Fast, J., and Berkowitz, C.: Photochemical age determinations in the Phoenix  
 706 metropolitan area, *J. Geophys. Res.*, 108, 4096, doi:10.1029/2002JD002621, 2003.

707 Krupa, S. V., Nosal, M., and Legge, A. H.: A numerical analysis of the combined open top chamber data from the  
 708 USA and Europe on ambient ozone and negative crop responses, *Environmental Pollution*, 101, 157–160, 1998.

709 Kumar, R., Naja, M., Venkataramani, S., and Wild, O.: Variations in surface ozone at Nainital: A high-altitude site  
 710 in the central Himalayas, *J. Geophys. Res.*, 115, D16302, doi:10.1029/2009JD013715, 2010.

711 Kumar, R., Naja, M., Pfister, G. G., Barth, M. C., and Brasseur, G. P.: Simulations over South Asia using the  
 712 Weather Research and Forecasting model with Chemistry (WRF-Chem): set-up and meteorological evaluation,  
 713 *Geoscientific Model Development*, 5, 321–343, 2012a.

714 Kumar, R., Naja, M., Pfister, G. G., Barth, M. C., Wiedinmyer, C., and Brasseur, G. P.: Simulations over South  
 715 Asia using the Weather Research and Forecasting model with Chemistry (WRF-Chem): chemistry evaluation and  
 716 initial results, *Geoscientific Model Development* 5, 619–648, 2012b.

717 Kumar, R., Barth, M. C., Pfister, G. G., Nair, V. S., Ghude, S. D., and Ojha, N.: What controls the seasonal cycle  
 718 of black carbon aerosols in India?, *J. Geophys. Res. Atmos.*, 120, 7788–7812, doi:10.1002/2015JD023298, 2015.

719 Lawrence, M. G., Rasch, P. J., von Kuhlmann, R., Williams, J., Fischer, H., de Reus, M., Lelieveld, J., Crutzen, P.  
 720 J., Schultz, M., Stier, P., Huntrieser, H., Heland, J., Stohl, A., Forster, C., Elbern, H., Jakobs, H., and Dickerson,  
 721 R. R.: Global chemical weather forecasts for field campaign planning: predictions and observations of large-scale  
 722 features during MINOS, CONTRACE, and INDOEX, *Atmos. Chem. Phys.*, 3, 267–289, doi:10.5194/acp-3-267-  
 723 2003, 2003.

724 Lawrence, M. G. and Lelieveld, J.: Atmospheric pollutant outflow from southern Asia: a review, *Atmos. chem.*  
 725 *Phys.*, 10, 11017–11096, doi:10.5194/acp-10-11017-2010, 2010.

726 Lelieveld, J., and Dentener, F.J.: What controls tropospheric ozone?, *J. Geophys. Res.*, 105, 3531-3551, 2000.

727 Lelieveld, J., Berresheim, H., Borrmann, S., Crutzen, P. J., Dentener, F. J., Fischer, H., Feichter, J., Flatau, P. J.,  
728 Heland, J., Holzinger, R., Korrmann, R., Lawrence, M. G., Levin, Z., Markowicz, K. M., Mihalopoulos, N.,  
729 Minikin, A., Ramanathan, V., de Reus, M., Roelofs, G. J., Scheeren, H. A., Sciare, J., Schlager, H., Schultz, M.,  
730 Siegmund, P., Steil, B., Stephanou, E. G., Stier, P., Traub, M., Warneke, C., Williams, J., and Ziereis, H.: Global  
731 air pollution crossroads over the Mediterranean, *Science*, 298, 794–799, doi:10.1126/science.1075457, 2002.

732 Lelieveld, J., Evans, J. S., Fnais, M., Giannadaki, D., and Pozzer, A.: The contribution of outdoor air pollution  
733 sources to premature mortality on a global scale, *Nature*, 525(7569):367-371, 2015.

734 Lin, Y.-L., R. D. Farley, R. D. and Orville, H. D.: Bulk parameterization of the snow field in a cloud model, *J.*  
735 *Clim. Appl. Meteorol.*, 22, 1065–1092, 1983.

736 Liu, Y., Warner, T. T., Bowers, J. F., Carson, L. P., Chen, F., Clough, C. A., Davis, C. A., Egeland, C. H.,  
737 Halvorson, S., Huck Jr., T. W., Lachapelle, L., Malone, R. E., Rife, D. L., Sheu, R., -S., Swerdlin, S. P. and  
738 Weingarten, D. S.: The operational mesogamma-scale analysis and forecast system of the U.S. Army Test and  
739 Evaluation Command. Part 1: Overview of the modeling system, the forecast products, *Journal of applied*  
740 *meteorology and climatology* 47, 1077–1092, 2008.

741 Logan, J. A., Staehelin, J., Megretskaia, I. A., Cammas, J.-P., Thouret, V., Claude, H., De Backer, H., Steinbacher,  
742 M., Scheel, H.-E., Stubi, R., Frohlich, M., and Derwent, R.: Changes in ozone over Europe: Analysis of ozone  
743 measurements from sondes, regular aircraft (MOZAIC) and alpine surface sites, *J. Geophys. Res.*, 117, D09301,  
744 doi:10.1029/2011JD016952, 2012.

745 Lu, Z. and Streets, D. G.: The Southeast Asia Composition, Cloud, Climate Coupling Regional Study Emission  
746 Inventory, available at: <http://bio.cgrer.uiowa.edu/SEAC4RS/emission.html>, 2012.

747 Lüthi, Z. L., Skerlak, B., Kim, S.-W., Lauer, A., Mues, A., Rupakheti, M., and Kang, S.: Atmospheric brown  
748 clouds reach the Tibetan Plateau by crossing the Himalayas, *Atmos. Chem. Phys.*, 15, 6007-6021,  
749 doi:10.5194/acp-15-6007-2015, 2015.

750 Mahapatra, P. S., Jena, J., Moharana, S., Srichandan, H., Das, T., Roy, C. G., and Das, S. N.: Surface ozone  
751 variation at Bhubaneswar and intra-corelationship study with various parameters, *J. Earth Syst. Sci.* 121, 1163–  
752 1175, 2012.

753 Mallik C., Lal, S., and Venkataramani, S.: Trace gases at a semi-arid urban site in western India: variability and  
754 inter-correlations, *J. Atm. Chem. Vol. 72*, p. 143-164, 2015.

755 Mar, K. A., Ojha, N., Pozzer, A., and Butler, T. M.: Ozone air quality simulations with WRF-Chem (v3.5.1) over  
756 Europe: model evaluation and chemical mechanism comparison, *Geosci. Model Dev.*, 9, 3699-3728,  
757 doi:10.5194/gmd-9-3699-2016, 2016.

758 Marrapu, P., Cheng, Y., Beig, G., Sahu, S. K., Srinivas, R. and Carmichael, G. R.: Air Quality in Delhi during the  
759 Commonwealth Games, *Atmos. Chem. Phys.*, 14:10619–10630, 2014.

760 Mellor, G. L., and Yamada, T.: Development of a turbulence closure model for geophysical fluid problems,  
761 *Reviews of geophysics and space physics* 20(4), 851–875, 1982.

762 Michael, M., Yadav, A., Tripathi, S. N., Kanawade, V. P., Gaur, A., Sadavarte, P. and Venkataraman, C.:  
763 Simulation of trace gases and aerosols over the Indian Domain: Evaluation of the WRF-Chem model, *Atmospheric*  
764 *Chemistry and Physics Discussion*, 13, 12287-12336, 2013.

765 Mlawer, E. J., Taubman, S. J., Brown, P. D., Iacono, M. J. and Clough, S. A.: Radiative transfer for  
766 inhomogeneous atmosphere: RRTM, a validated correlated-k model for the long-wave, *Journal of Geophysical*  
767 *Research* 102 (D14), 16663–16682, 1997.

768 Monin, A. S. and Obukhov, A. M.: Basic laws of turbulent mixing in the surface layer of the atmosphere, *Contrib.*  
769 *Geophys. Inst. Acad. Sci., USSR* 24 (151), 163–187, 1954.

770 Monks, P. S., Archibald, A. T., Colette, A., Cooper, O., Coyle, M., Derwent, R., Fowler, D., Granier, C., Law, K.  
771 S., Mills, G. E., Stevenson, D. S., Tarasova, O., Thouret, V., von Schneidm  sser, E., Sommariva, R., Wild, O.,  
772 and Williams, M. L.: Tropospheric ozone and its precursors from the urban to the global scale from air quality to  
773 short-lived climate forcer, *Atmos. Chem. Phys.*, 15, 8889-8973, doi:10.5194/acp-15-8889-2015, 2015.

774 Nishanth, T., Praseed, K. M., Satheesh Kumar, M. K., and Valsaraj, K. T.: Analysis of Ground Level O<sub>3</sub> and NO<sub>x</sub>  
775 Measured at Kannur, India. *J Earth Sci Climate Change*, 3:111, doi:10.4172/2157-7617.1000111, 2012.

776 Ohara, T., Akimoto, H., Kurokawa, J., Horii, N., Yamaji, K., Yan, X., and Hayasaka, T.: An Asian emission  
777 inventory of anthropogenic emission sources for the period 1980–2020, *Atmos. Chem. Phys.*, 7, 4419–4444,  
778 doi:10.5194/acp-7-4419-2007, 2007.

779 Ojha, N., Naja, M., Singh, K. P., Sarangi, T., Kumar, R., Lal, S., Lawrence, M. G., Butler, T. M., and Chandola,  
780 H. C.: Variabilities in ozone at a semi-urban site in the Indo-Gangetic Plain region: Association with the  
781 meteorology and regional process, *J. Geophys. Res.*, 117, D20301, doi:10.1029/2012JD017716, 2012.

782 Ojha, N., Naja, M., Sarangi, T., Kumar, R., Bhardwaj, P., Lal, S., Venkataramani, S., Sagar, R., Kumar, A., and  
783 Chandola, H. C.: On the processes influencing the vertical distribution of ozone over the central Himalayas:  
784 Analysis of yearlong ozonesonde observations, *Atmos. Environ.*, 88, 201–211,  
785 doi:10.1016/j.atmosenv.2014.01.031, 2014.

786 Ojha, N., Pozzer, A., Rauthe-Sch  ch, A., Baker, A. K., Yoon, J., Brenninkm  ijer, C. A. M., and Lelieveld, J.:  
787 Ozone and carbon monoxide over India during the summer monsoon: regional emissions and transport, *Atmos.*  
788 *Chem. Phys.*, 16, 3013-3032, doi:10.5194/acp-16-3013-2016, 2016.

789 Otte, T. L.: The impact of nudging in the meteorological model for retrospective air quality simulations. Part I:  
790 Evaluation against national observation networks, *J. Appl. Meteor. Climatol.*, 47, 1853–1867, 2008.

791 Pozzer, A., Zimmermann, P., Doering, U. M., van Aardenne, J., Tost, H., Dentener, F., Janssens-Maenhout, G.,  
792 and Lelieveld, J.: Effects of business-as-usual anthropogenic emissions on air quality, *Atmos. Chem. Phys.*, 12,  
793 6915-6937, doi:10.5194/acp-12-6915-2012, 2012.

794 Reddy, B. S. K., Kumar, K. R., Balakrishnaiah, G., Gopal, K. R., Reddy, R. R., Ahammed, Y. N., Narasimhulu,  
795 K., Reddy, L. S. S., and Lal, S.: Observational studies on the variations in surface ozone concentration at  
796 Anantapur in southern India, *Atmos. Res.* 98, 125–139, 2010.

797 Renuka, K., Gadhavi, H., Jayaraman, A., Lal, S., Naja, M., and Rao, S.: Study of Ozone and NO<sub>2</sub> over Gadanki –  
798 a rural site in South India, *J. Atmos. Chem.*, 71, 95–112, doi:10.1007/s10874-014-9284-y, 2014.

799 Sarangi, T., Naja, M., Ojha, N., Kumar, R., Lal, S., Venkataramani, S., Kumar, A., Sagar, R., and Chandola, H. C.:  
800 First simultaneous measurements of ozone, CO and NO<sub>y</sub> at a high altitude regional representative site in the  
801 central Himalayas, *J. Geophys. Res.-Atmos.*, 119, 1592–1611, doi:10.1002/2013JD020631, 2014.

802 Sarkar, M., Venkataraman, C., Guttikunda, S., and Sadavarte, P.: Indian emissions of technology-linked NMVOCs  
803 with chemical speciation: An evaluation of the SAPRC99 mechanism with WRF-CAMx simulations, *Atmospheric*  
804 *Environment*, 134, 70-83, <http://dx.doi.org/10.1016/j.atmosenv.2016.03.037>, 2016.

805 Sarkar, S., Srivastava, R. K., and Sagar, K.: Diurnal Monitoring Of Surface Ozone And PM<sub>2.5</sub> Concentration  
806 And Its Correlation With Temperature, *INTERNATIONAL JOURNAL OF TECHNOLOGY ENHANCEMENTS*  
807 *AND EMERGING ENGINEERING RESEARCH*, VOL 3, ISSUE 09, ISSN 2347-4289, 2015.

808 Schell, B., Ackermann, I. J., Hass, H., Binkowski, F. S., and Ebel, A.: Modeling the formation of secondary  
809 organic aerosol within a comprehensive air quality model system, *J. Geophys. Res.-Atmos.*, 106, 28275–28293,  
810 doi:10.1029/2001JD000384, 2001.

811 Sillman, S.: The use of NO<sub>y</sub>, H<sub>2</sub>O<sub>2</sub> and HNO<sub>3</sub> as indicators for ozone-NO<sub>x</sub>-hydrocarbon sensitivity in urban  
812 locations, *J. Geophys. Res.*, 100, 14175–14188, 1995.

813 Sinha, V., Kumar, V., and Sarkar, C.: Chemical composition of pre-monsoon air in the Indo-Gangetic Plain  
814 measured using a new PTR-MS and air quality facility: high surface ozone and strong influence of biomass  
815 burning, *Atmos. Chem. Phys.*, 14, 5921-5941, 2014.

816 Stauffer, D. R., and Seaman, N. L.: Use of four-dimensional data assimilation in a limited area mesoscale model.  
817 Part I: Experiments with synoptic-scale data, *Monthly Weather Review* 118, 1250- 1277, 1990.

818 Stauffer, D. R., Seaman, N. L. and Binkowski, F. S.: Use of four-dimensional data assimilation in a limited-area  
819 mesoscale model. Part II: Effects of data assimilation within the planetary boundary layer, *Monthly Weather*  
820 *Review* 119, 734-754, 1991.

821 Stockwell, W. R., Middleton, P., Chang, J. S., and Tang, X.: The second generation regional Acid Deposition  
822 Model chemical mechanism for regional air quality modeling, *J. Geophys. Res.*, 95, 16343-16367, 1990.

823 Taylor, K. E.: Summarizing multiple aspects of model performance in a single diagram, *J. Geophys. Res.* 106:  
824 7183–7192, 2001.

825 Tewari, M., Chen, F., Wang, W., Dudhia, J., Lemone, M. A., Mitchell, K. E., Ek, M., Gayno, G., Wegiel, J. W.  
826 and Cuenca, R.: Implementation and verification of the unified Noah land-surface model in the WRF model, 20th

827 Conference on Weather Analysis and Forecasting/16th Conference on Numerical Weather Prediction, Seattle,  
828 WA, American Meteorological Society, 2004.

829 Tie, X., Geng, F., Guenther, A., Cao, J., Greenberg, J., Zhang, R., Apel, E., Li, G., Weinheimer, A., Chen, J., and  
830 Cai, C.: Megacity impacts on regional ozone formation: observations and WRF-Chem modeling for the MIRA GE-  
831 Shanghai field campaign, *Atmos. Chem. Phys.*, 13, 5655-5669, <https://doi.org/10.5194/acp-13-5655-2013>, 2013.

832 Wiedinmyer, C., Akagi, S. K., Yokelson, R. J., Emmons, L. K., Al-Saadi, J. A., Orlando, J. J., and Soja, A. J.: The  
833 Fire INventory from NCAR (FINN): a high resolution global model to estimate the emissions from open burning,  
834 *Geosci. Model Dev.*, 4, 625–641, doi:10.5194/gmd-4-625-2011, 2011.

835 Wild, O., Zhu, X. and Prather, M. J.: Fast-J: Accurate simulation of in- and below cloud photolysis in tropospheric  
836 chemical models, *Journal of Atmospheric Chemistry*, 37, 245-282, 2000.

837 Wilkinson, S., Mills, G., Illidge, R., and Davies, W. J.: How is ozone pollution reducing our food supply?, *J. Exp.*  
838 *Bot.*, 63, 527–536, doi:10.1093/jxb/err317, 2012.

839 Yadav, R., Sahu, L. K., Jaaffrey, S. N. A., and Beig, G.: Distributions of ozone and related trace gases at an urban  
840 site in western India. *J. Atmos. Chem.* 71, 125–144, 2014.

841 Yang, M., Howell, S. G., Zhuang, J., and Huebert, B. J.: Attribution of aerosol light absorption to black carbon,  
842 brown carbon, and dust in China – interpretations of atmospheric measurements during EAST-AIRE, *Atmos.*  
843 *Chem. Phys.*, 9, 2035–2050, doi:10.5194/acp-9-2035-2009, 2009.

844 Yoon, J. and Pozzer, A.: Model-simulated trend of surface carbon monoxide for the 2001–2010 decade, *Atmos.*  
845 *Chem. Phys.*, 14, 10465-10482, doi:10.5194/acp-14-10465-2014, 2014.

846 Zanis, P., Hadjinicolaou, P., Pozzer, A., Tyrllis, E., Dafka, S., Mihalopoulos, N., and Lelieveld, J.: Summertime  
847 free-tropospheric ozone pool over the eastern Mediterranean/Middle East, *Atmos. Chem. Phys.*, 14, 115-132,  
848 doi:10.5194/acp-14-115-2014, 2014.

849 Zaveri, R. A. and Peters, L. K.: A new lumped structure photochemical mechanism for large-scale applications,  
850 *JOURNAL OF GEOPHYSICAL RESEARCH*, VOL. 104, NO. D23, PAGES 30387-30415, 1999.

851 Zhang, Q., Streets, D. G., Carmichael, G. R., He, K. B., Huo, H., Kannari, A., Klimont, Z., Park, I. S., Reddy, S.,  
852 Fu, J. S., Chen, D., Duan, L., Lei, Y., Wang, L. T., and Yao, Z. L.: Asian emissions in 2006 for the NASA  
853 INTEX-B mission, *Atmos. Chem. Phys.*, 9, 5131–5153, doi:10.5194/acp-9-5131-2009, 2009.

854

855

856

857

858

859 **Table 1.** Abbreviations/ Acronym

|          |  |
|----------|--|
| EDGAR    | Emission Database for Global Atmospheric Research                  |
| HTAP     | Hemispheric Transport of Air Pollution                             |
| IGP      | Indo Gangetic plain  |
| IST      | Indian standard time   |
| INTEX-B  | Intercontinental Chemical Transport Experiment Phase B             |
| MB       | Mean Bias  |
| MOZART   | Model for Ozone and Related Chemical Tracers                       |
| NMB      | Normalized mean bias   |
| PBL      | Planetary boundary layer   |
| RMSD     | Centered root mean squared difference                              |
| RRTM     | Rapid Radiative Transfer Model                                     |
| SEAC4RS  | Southeast Asia Composition, Cloud, Climate Coupling Regional Study |
| WRF-Chem | Weather research and forecasting model coupled with chemistry      |

860

861

862 **Table 2.** Sub-regional estimates of anthropogenic emissions (in million mol h<sup>-1</sup>) in the three emission inventories  
863 used.

| Region  | HTAP            |       |       | INTEX-B         |       |       | SEAC4RS         |       |      |
|---------|-----------------|-------|-------|-----------------|-------|-------|-----------------|-------|------|
|         | NO <sub>x</sub> | NMVOC | CO    | NO <sub>x</sub> | NMVOC | CO    | NO <sub>x</sub> | NMVOC | CO   |
| North   | 8.1             | 14.0  | 110.0 | 6.3             | 10.0  | 96.1  | 8.7             | 10.7  | 86.9 |
| East    | 5.8             | 10.1  | 102.9 | 6.0             | 6.9   | 78.8  | 6.7             | 8.2   | 72.4 |
| West    | 2.9             | 4.6   | 31.0  | 1.8             | 2.1   | 24.7  | 3.7             | 2.9   | 24.3 |
| Central | 4.6             | 4.2   | 44.6  | 2.0             | 2.9   | 34.7  | 4.9             | 3.1   | 26.2 |
| South   | 5.4             | 5.8   | 37.2  | 2.7             | 4.1   | 46.2  | 3.5             | 3.4   | 28.3 |
| Total   | 26.8            | 38.7  | 325.7 | 18.8            | 26.0  | 280.5 | 27.5            | 28.3  | 238  |

864

865

866 **Table 3.** A brief description of the different WRF-Chem simulations conducted.

| Sr. No. | Simulation name | Emission Inventory | Year of Emission Inventory | Spatial Resolution of Emission Inventory | Chemical Mechanism |
|---------|-----------------|--------------------|----------------------------|--|--------------------|
| 1       | HTAP-RADM2      | HTAP               | 2010                       | 0.1°x 0.1°                               | RADM2              |
| 2       | INTEX-RADM2     | INTEX-B            | 2006                       | 0.5°x 0.5°                               | RADM2              |
| 3       | S4RS-RADM2      | SEAC4RS            | 2012                       | 0.1°x 0.1°                               | RADM2              |
| 4       | HTAP-MOZ        | HTAP               | 2010                       | 0.1°x 0.1°                               | MOZART-4           |

867

868

869

870

871

872

873

874



**Table 4.** List of observation sites and data sources used. Site nomenclature in brackets in column 1 is used in figures 1, 5, 6, 9 and 10.

| Site                    | Type           | Latitude | Longitude | Altitude<br>(m.a.s.l.) | Data period     | Reference                      |
|-------------------------|----------------|----------|-----------|------------------------|-----------------|--------------------------------|
| Mohali (MOH)            | Urban          | 30.7°N   | 76.7°N    | 310                    | May 2012        | Sinha et al. (2014)            |
| Nainital (NTL)          | Highly complex | 29.37°N  | 79.45°E   | 1958                   | Apr 2011        | Saranghi et. al. (2014)        |
| Pantnagar (PNT)         | Urban/complex  | 29.0°N   | 79.5°E    | 231                    | Apr 2009-11     | Ojha et al. (2012)             |
| Delhi (DEL)             | Urban          | 28.65°N  | 77.27°E   | 220                    | Apr 2013        | SAFAR data                     |
| Dibrugarh (DBG)         | Rural/complex  | 27.4°N   | 94.9°E    | 111                    | Apr 2010-13     | Bhuyan et al. (2014)           |
| Kanpur (KNP)            | Urban          | 26.46°N  | 80.33°E   | 125                    | Mar-May 2010-13 | Gaur et al. (2014)             |
| Udaipur (UDP)           | Urban          | 24.58°N  | 73.68°E   | 598                    | Apr 2010        | Yadav et al. (2014)            |
| Jabalpur (JBL)          | Complex        | 23.17°N  | 79.92°E   | 411                    | Apr 2013        | Sarkar et al. (2015)           |
| Ahmedabad (ABD)         | Urban          | 23.03°N  | 72.58°E   | 53                     | May 2011        | Mallik et al. (2015)           |
| Bhubaneswar (BBR)       | Urban          | 21.25°N  | 85.25°E   | 45                     | Mar-May 2010    | Mahapatra et al. (2012)        |
| Pune (PUN)              | Urban          | 18.54°N  | 73.81°E   | 559                    | Mar-May 2013    | SAFAR data; Beig et al. (2007) |
| Anantapur (ANP)         | Rural          | 14.62°N  | 77.65°E   | 331                    | Apr 2009        | Reddy et al. (2010)            |
| Gadanki (GDK)           | Rural          | 13.48°N  | 79.18°E   | 375                    | Mar-May 2010-11 | Renuka et al. (2014)           |
| Kannur (KNR)            | Rural/coastal  | 11.9°N   | 75.4°E    | 5                      | Apr 2010        | Nishanth et al. (2012)         |
| Thumba/Trivendrum (TRI) | Urban/coastal  | 8.55°N   | 77°E      | 3                      | Apr 2009        | David et al. (2011)            |

\* At Darjeeling only monthly mean value is available.

**Table 5.** A comparison of correlation coefficients (r) over different regions for the four simulations

| Region  | HTAP-RADM2 | INTEX-RADM2 | S4RS-RADM2 | HTAP-MOZ |
|---------|------------|-------------|------------|----------|
| North   | 0.90       | 0.86        | 0.88       | 0.90     |
| East    | 0.98       | 0.97        | 0.97       | 0.98     |
| West    | 0.99       | 0.98        | 0.98       | 0.99     |
| Central | 0.70       | 0.67        | 0.69       | 0.75     |
| South   | 0.99       | 0.98        | 0.97       | 0.97     |
| Overall | 0.98       | 0.97        | 0.97       | 0.99     |

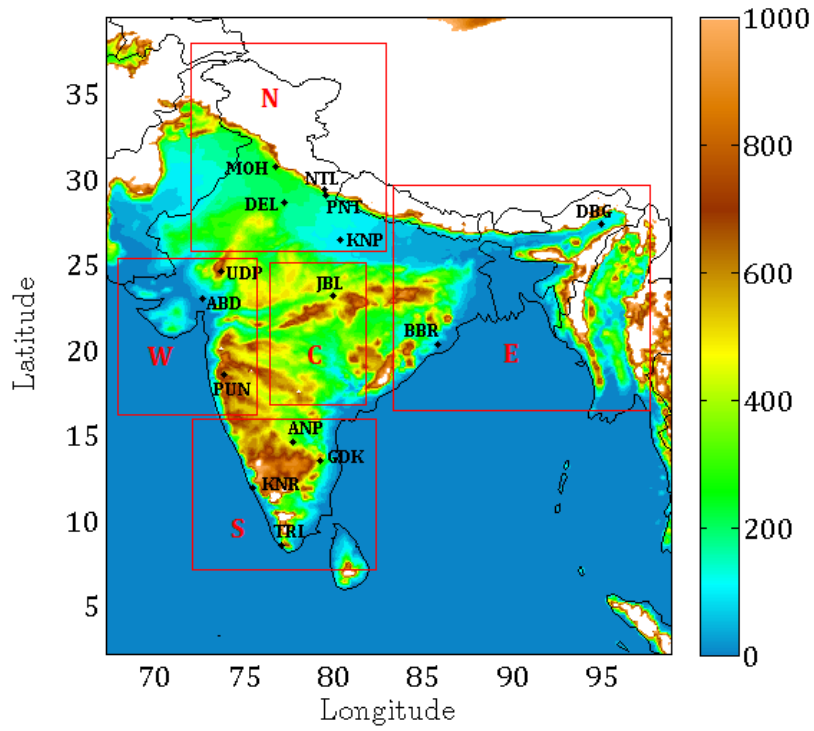


**Figure 1.** Simulation domain showing terrain height (in metres) and observation sites. White region indicates that the terrain height is equal to or exceeds 1 km. The domain is subdivided into five regions viz. North (N), South (S), East (E), West (W) and central (C) regions, as shown by red rectangles.

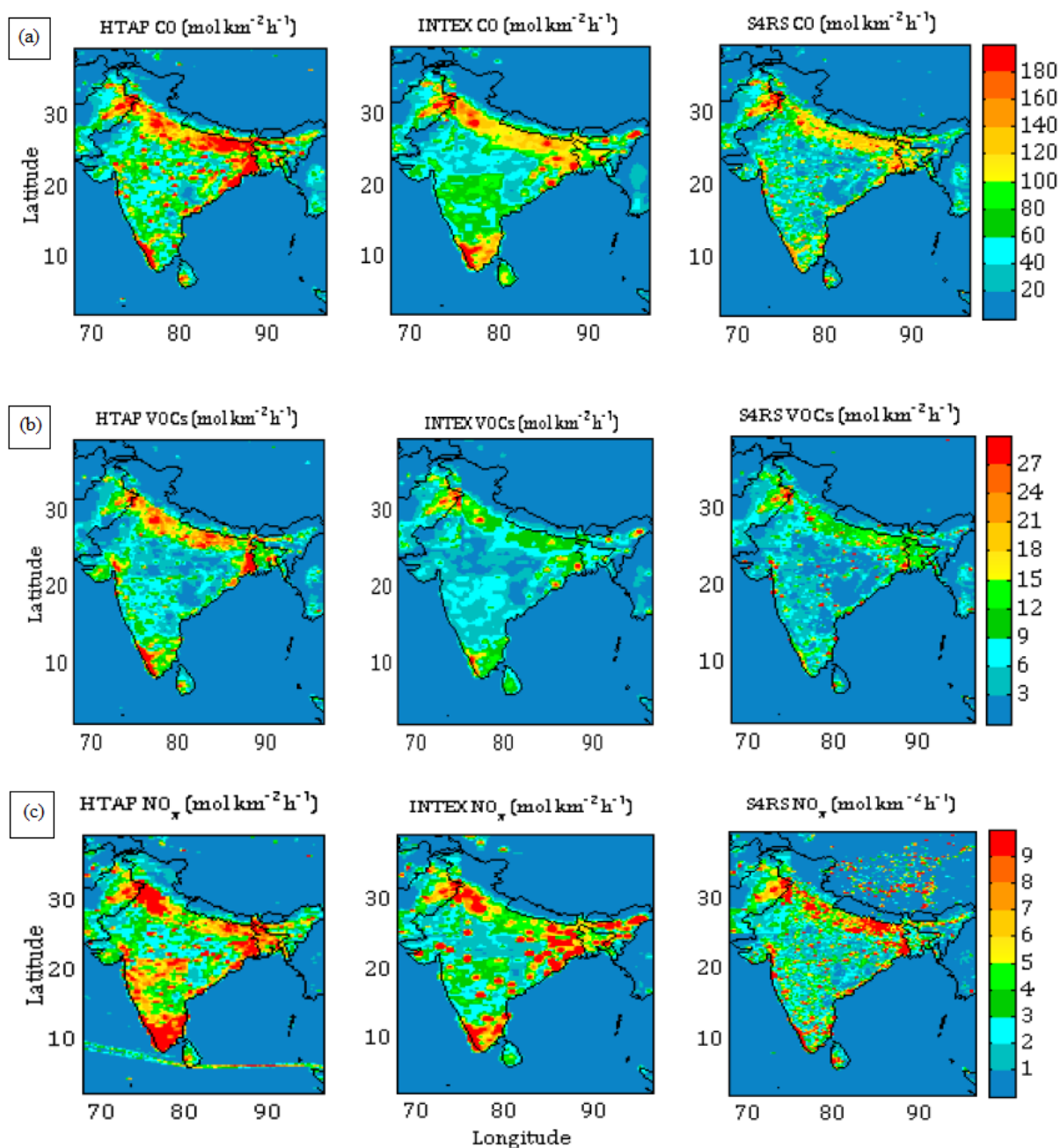


**Figure 2.** Comparison of (a) CO, (b) NM VOC and (c) NO<sub>x</sub> emissions between the three inventories used (see Section-2.2 for description).

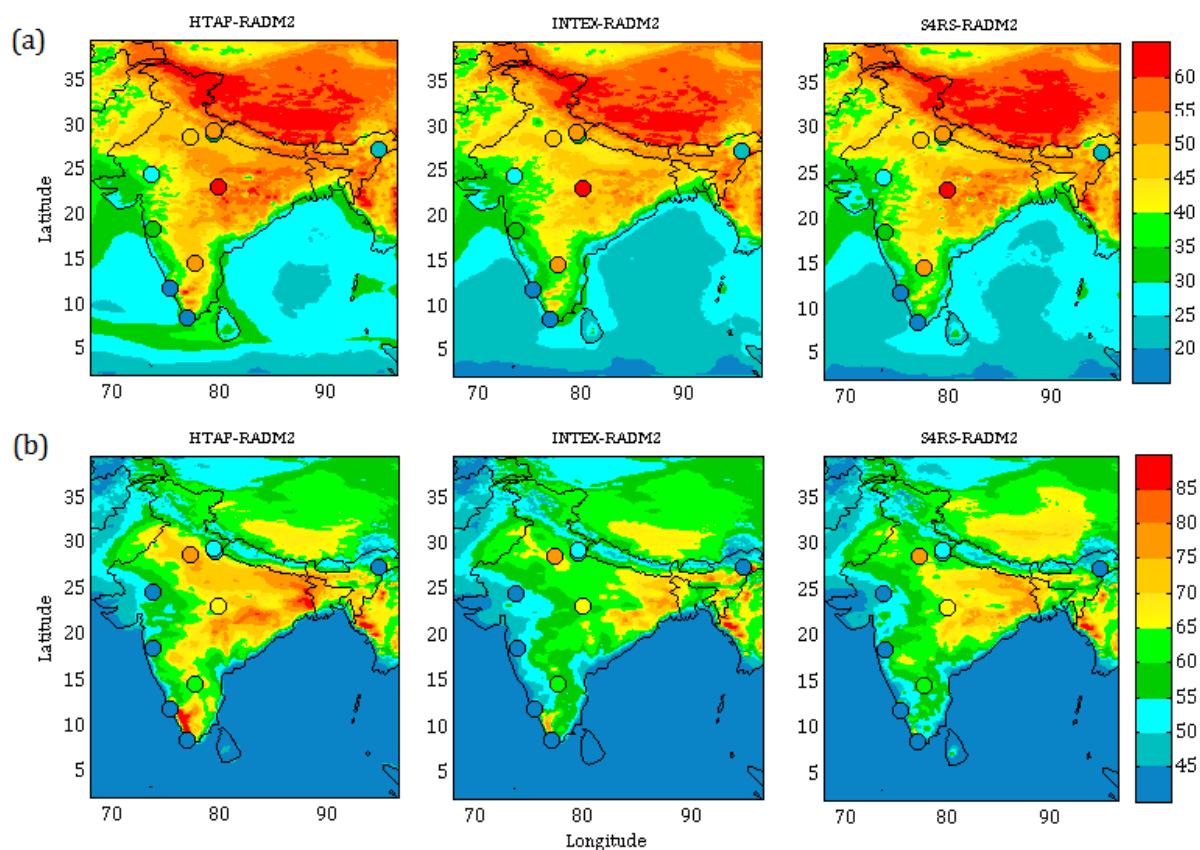


**Figure 3.** Monthly (April) average surface ozone calculated for (a) 24 h and (b) noontime (1130-1630 IST). The average ozone mixing ratios (ppbv) from observations are also shown for comparison on the same colour scale. Note the difference in colour scales in the top and bottom rows.

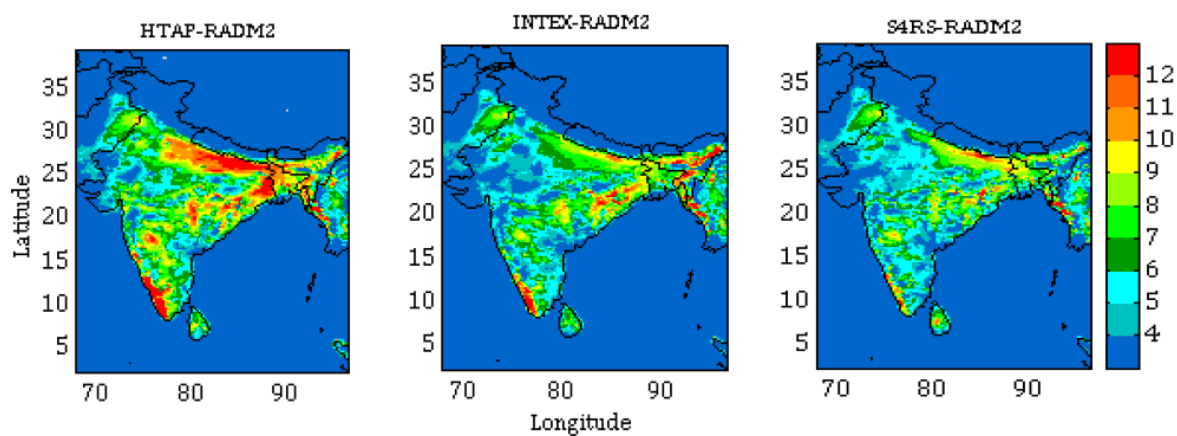


**Figure 4.** Net daytime surface ozone chemical tendency (in ppbv h<sup>-1</sup>) for the month April during 0630-1230 IST.

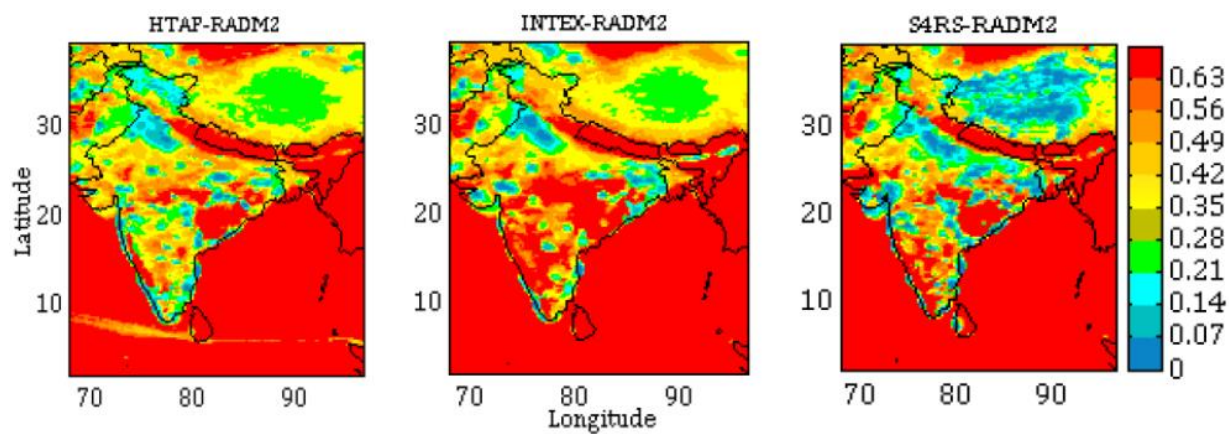


**Figure 5.** Net daytime surface  $\text{CH}_2\text{O}$  to  $\text{NO}_y$  ratio in simulations with different inventories for the month April during 0630-1230 IST.

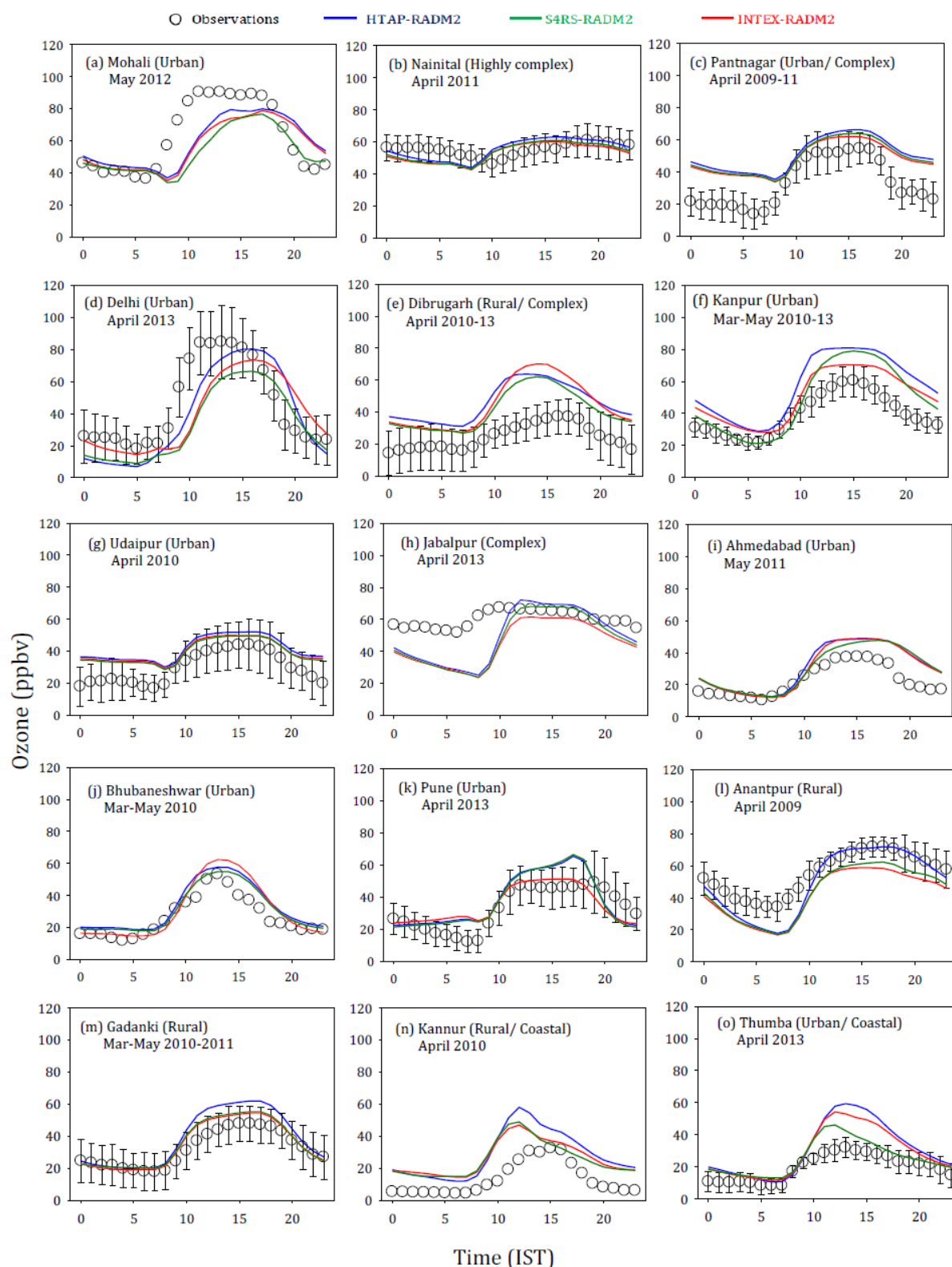
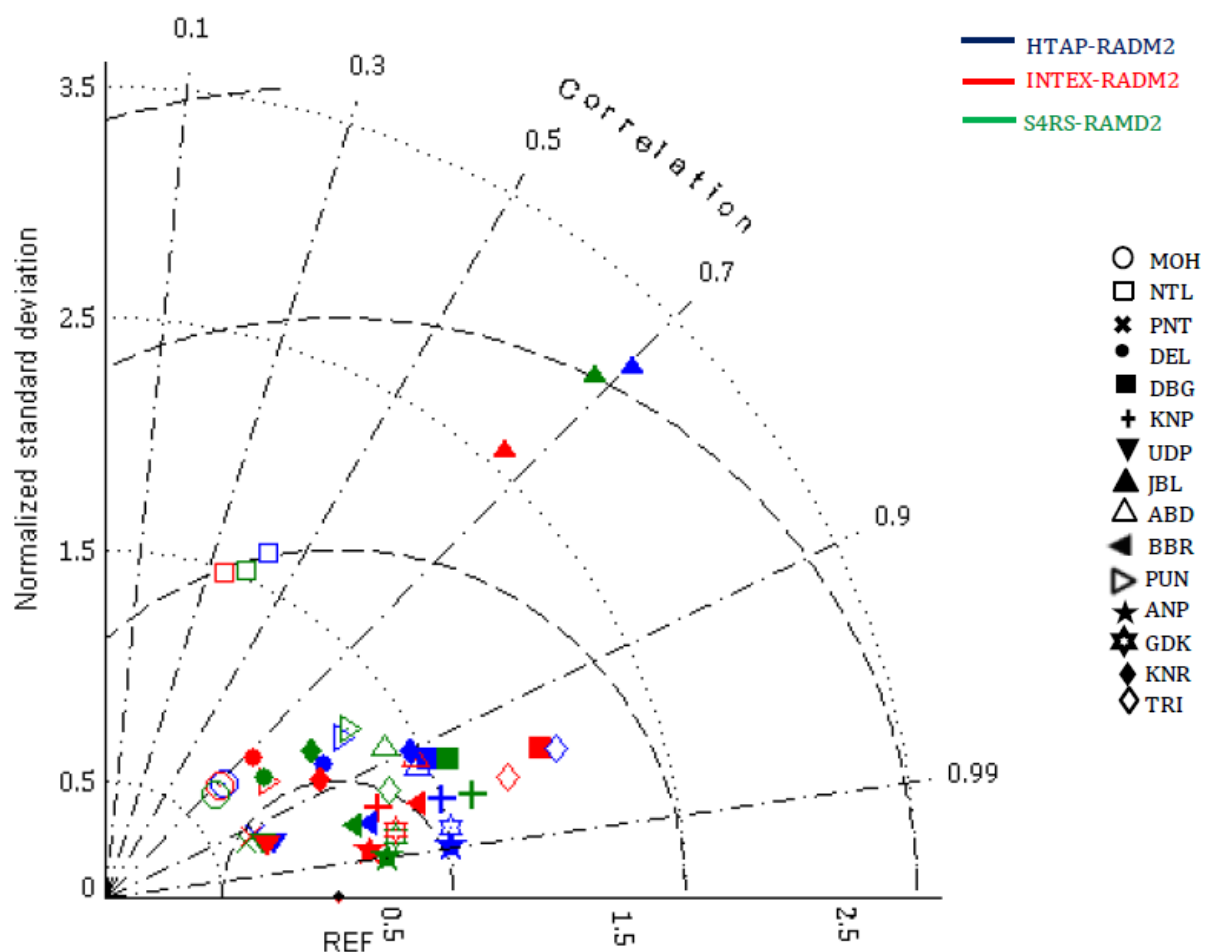


**Figure 6.** Comparison of monthly average diurnal variation of surface ozone simulated using different emission inventories at various observation sites. The observational data is available for the period indicated in the figure whereas all model simulations are for the year 2013. Error bars represent the temporal standard deviations of the monthly averages. All model simulations are with RADM2 chemistry.



973  
 974 **Figure 7.** Taylor diagram with summary model statistics ( $r$ , normalized standard deviation and RMSD) at all sites. The  
 975 correlation is the cosine of the angle from the horizontal axis, the root mean square difference is the distance from the reference  
 976 point (REF) and the standard deviation is the distance from the origin.



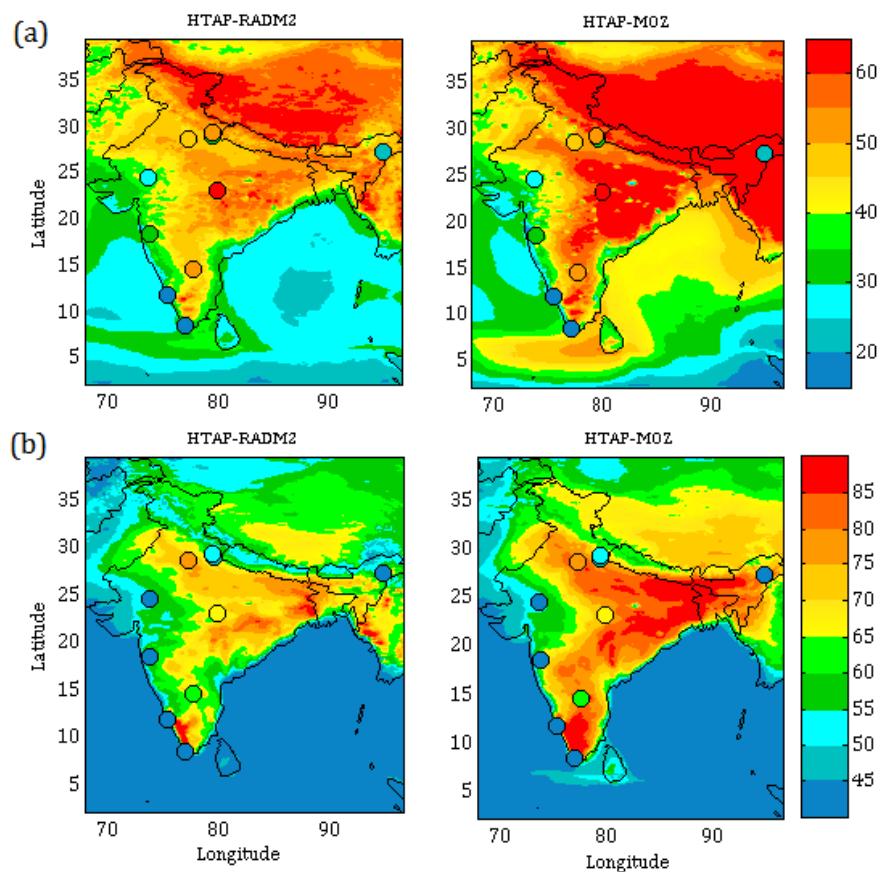


**Figure 8.** Monthly (April) average surface ozone calculated for (a) 24 h and (b) noontime (1130-1630 IST), comparing the chemical mechanisms (RADM2 and MOZART). The average ozone mixing ratios (ppbv) from observations are also shown for comparison on the same colour scale. Note the difference in colour scales in the top and bottom rows.

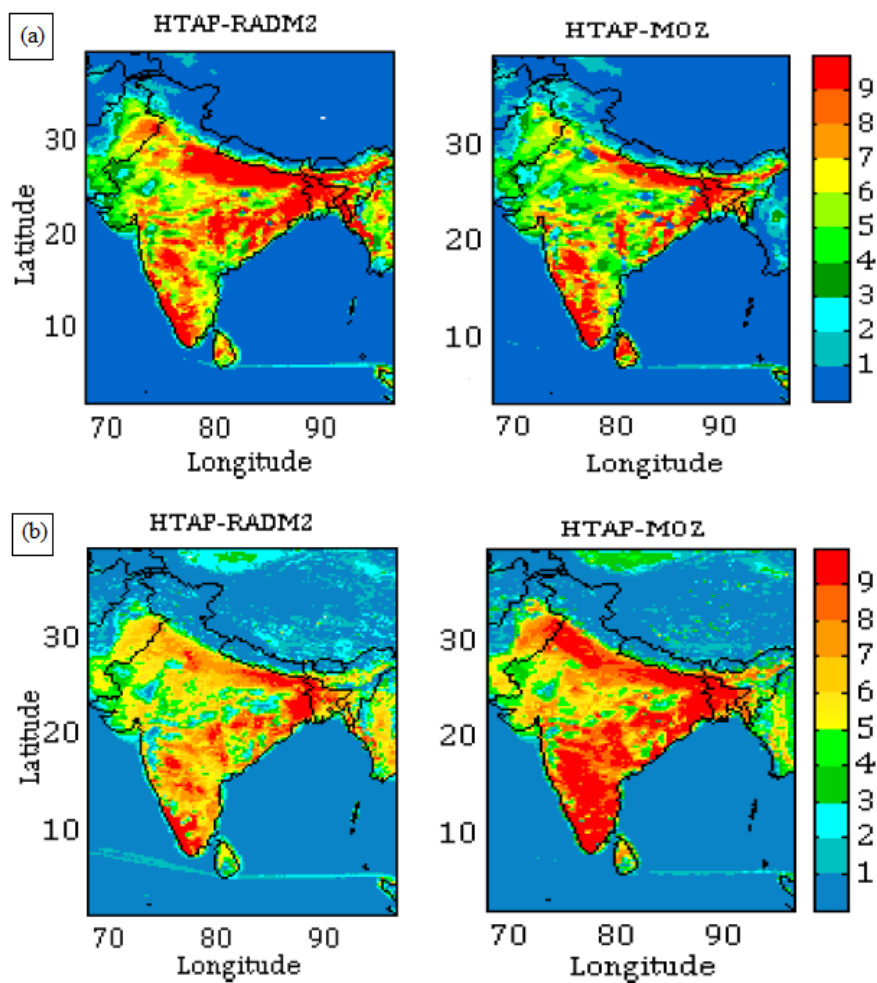


**Figure 9.** Average (a) net daytime surface ozone chemical tendency (in ppbv h<sup>-1</sup>) (b) net daytime surface ozone chemical +vertical mixing tendency (in ppbv h<sup>-1</sup>) for April during 0630-1230 IST

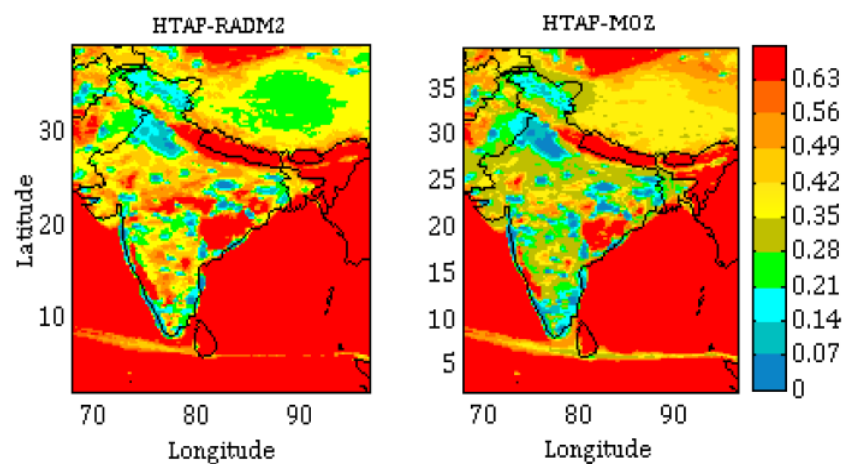


**Figure 10.** Net daytime surface  $\text{CH}_2\text{O}$  to  $\text{NO}_y$  ratio in simulations with different chemical mechanisms for the month April during 0630-1230 IST.

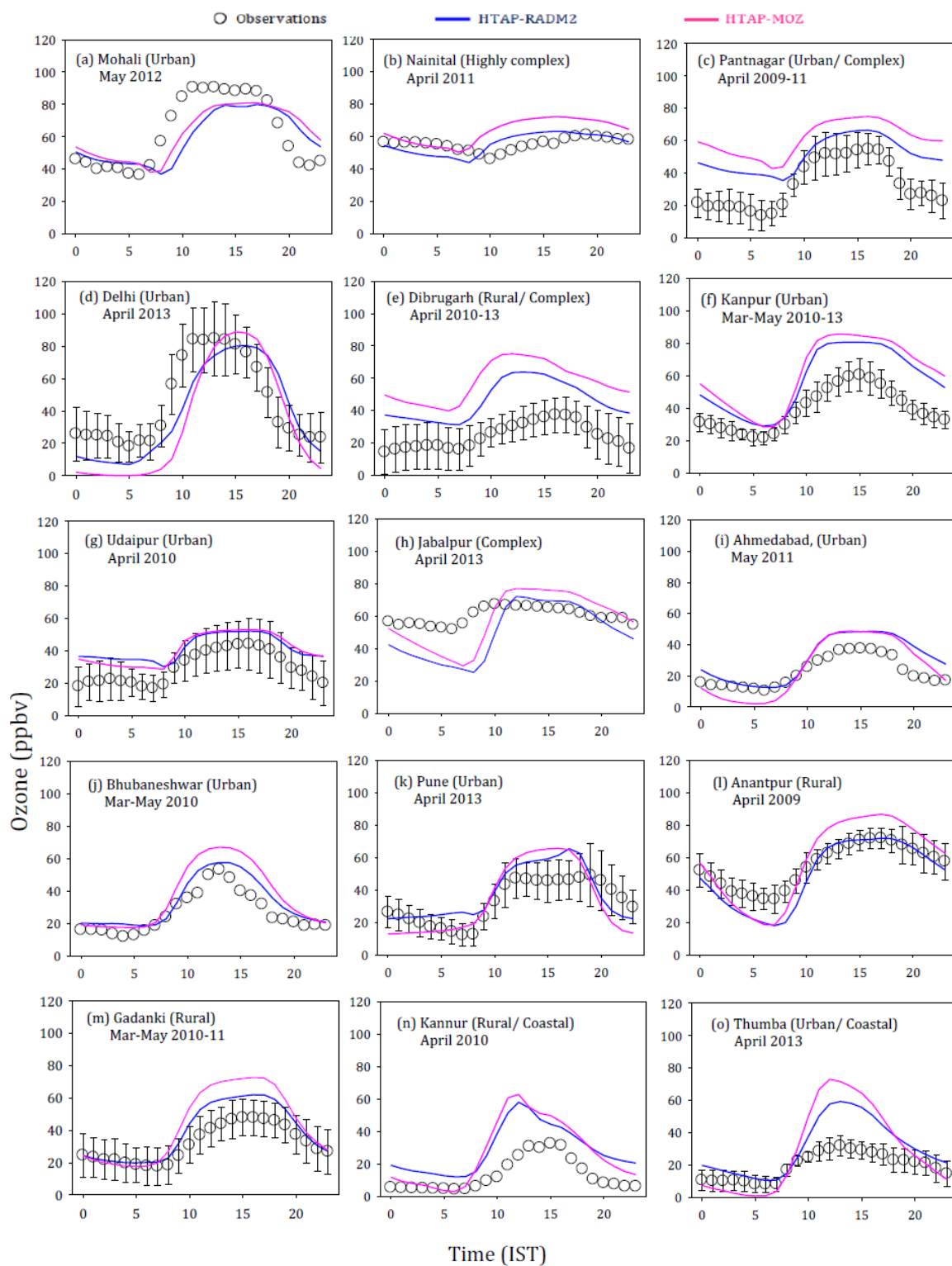
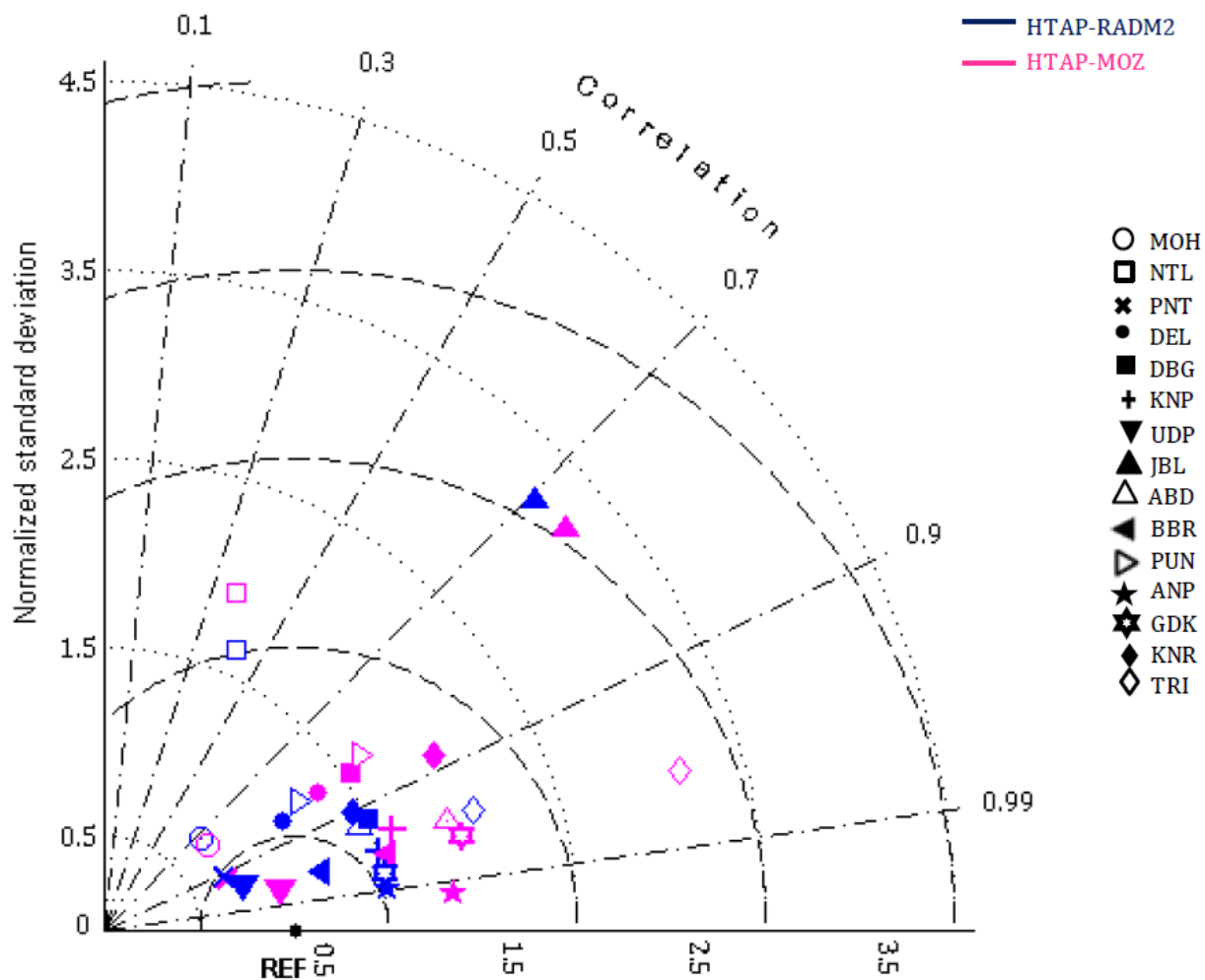


**Figure 11.** Comparison of monthly average diurnal variation of surface ozone simulated using different chemical mechanisms at various observation sites. The observational data is available for the period indicated in the figure whereas all the model simulations are for the year 2013. Error bars represent the temporal standard deviations of the monthly averages. All model simulations are with the HTAP inventory.



1030  
 1031 **Figure 12.** Taylor diagram with summary model statistics ( $r$ , normalized standard deviation and RMSD) at all sites. The  
 1032 correlation is the cosine of the angle from the horizontal axis, the root mean square difference is the distance from the reference  
 1033 point (REF) and the standard deviation is the distance from the origin.

1034  
 1035  
 1036  
 1037  
 1038  
 1039  
 1040  
 1041  
 1042  
 1043  
 1044  
 1045  
 1046

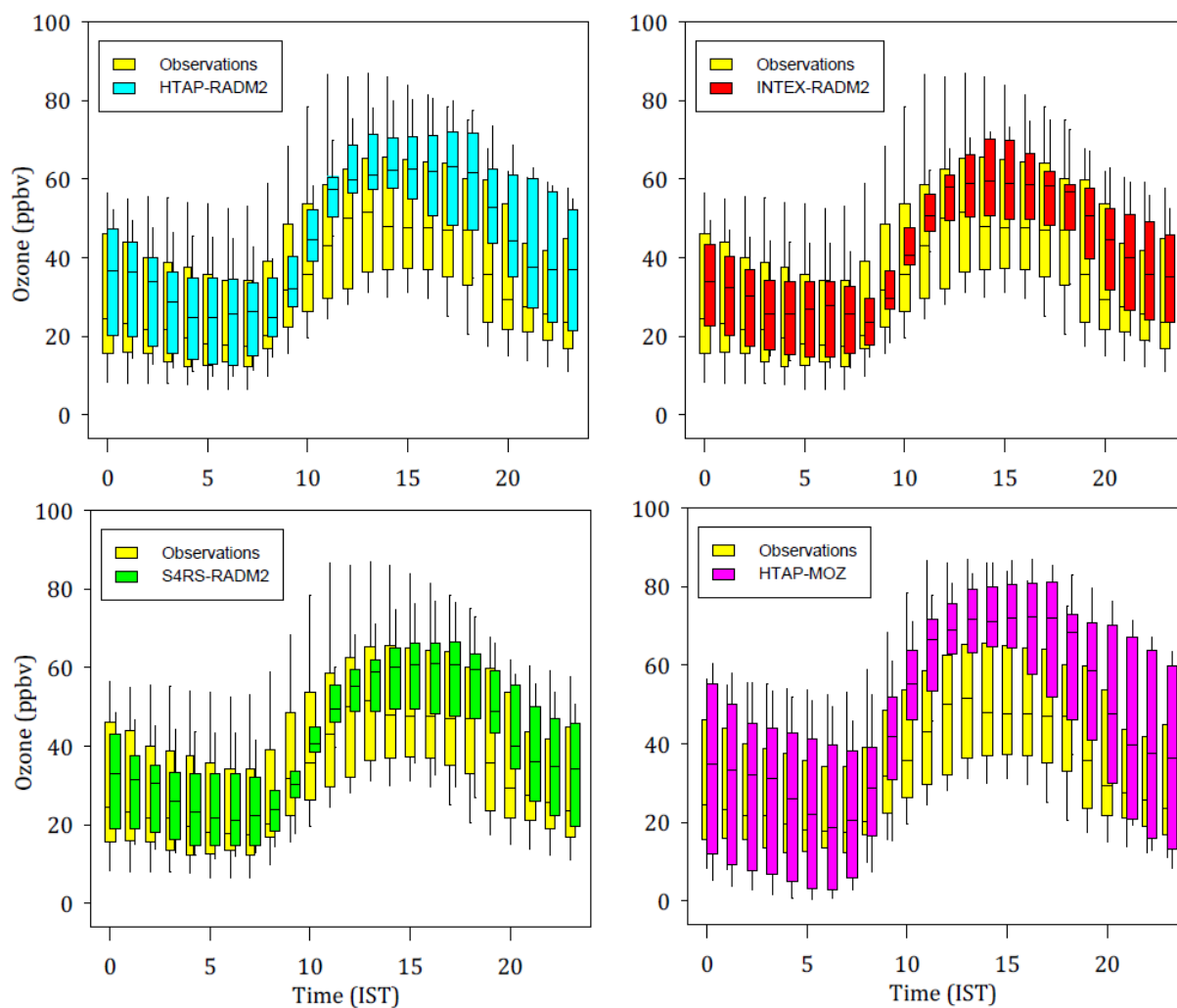


**Figure 13.** Box/whisker plot comparison of monthly average diurnal variation of surface ozone from model runs and observations over the entire domain (after spatially averaging the results). Upper and lower boundaries of boxes denote the 75th and 25th percentiles and whiskers represent the 95th and 5th percentiles. The line in the box is the median.

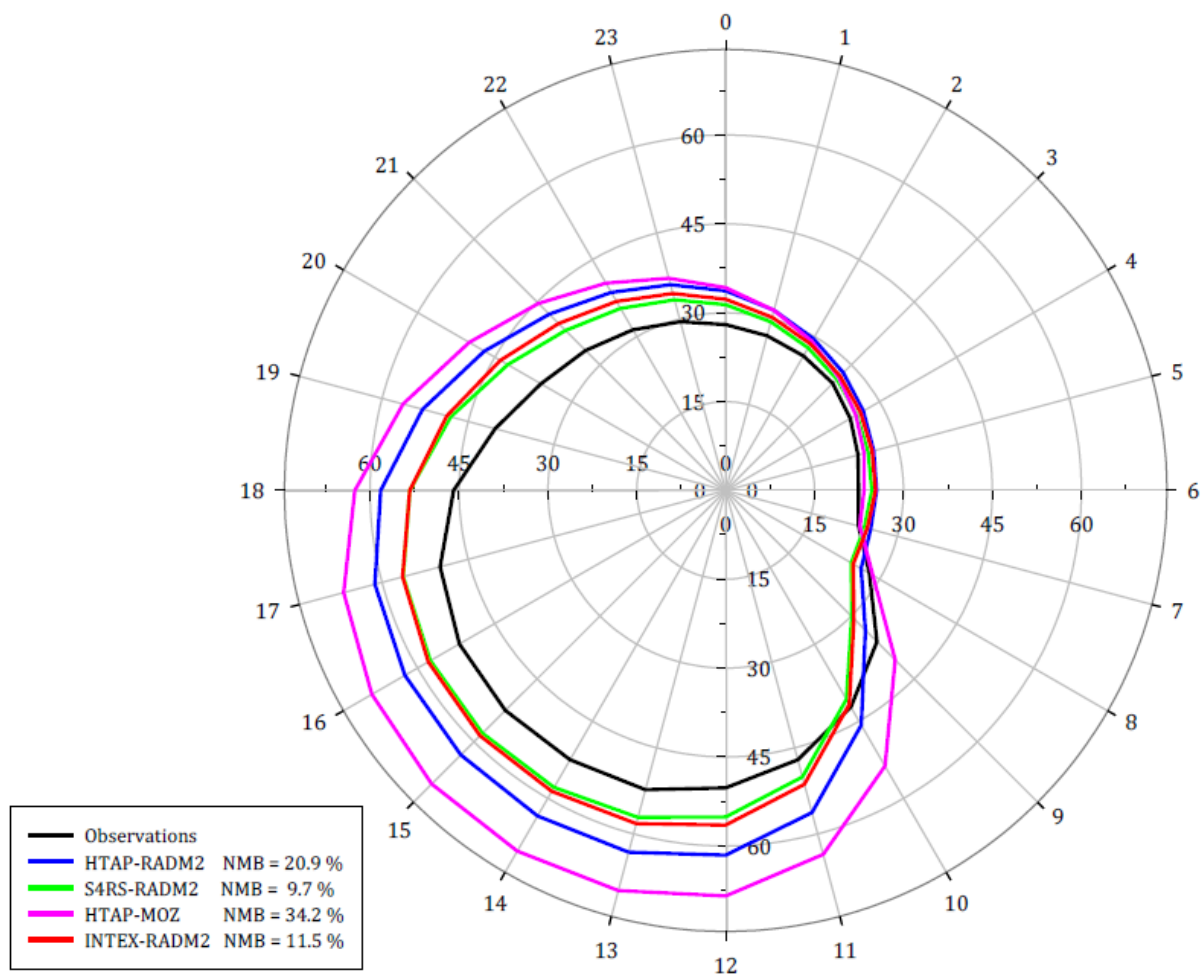


**Figure 14.** Polar plot for monthly mean diurnal variation of surface ozone (in ppbv) from all model simulations and observations each spatially averaged over all sites. The numbers on the outermost circle represent the hour of the day and the radial distance from the centre represents surface ozone mixing ratios in ppbv. The normalized mean biases (NMB in %) for noontime surface ozone are indicated in the caption box.